Complex Embedded Automotive Control Systems
CEmACS

DaimlerChrysler
SINTEF
Glasgow University
Hamilton Institute
Lund University

Public
Final Report Workpart 3
Controller Design
Deliverable D15

September 2006

Executive Summary

This is the final report of work package 3 (WP 3 *Controller Design*) of the CEMACS project (deliverable D15). It covers the 24 months of activities towards Milestone 3.

The focus of work package 3 is on the theory and methods of controller design with the aim to adapt these to the applicational needs of the project. The expected result for Milestone 3 is a consolidated framework of design methods after practical evaluation. The developed algorithms have been implemented in software and are being made available to activities in other workparts.

Consequently, this report focuses on the specific design methods as they relate to the applications in the work packages 1 (*Vehicle control for active safety*) and 2 (*Integrated Chassis control / Generic prototype*).

Most project partners have been active in this work package during the reporting period. This can be summarised as follows: SINTEF has worked on WP 3.2 (Hybrid Control Systems) and WP 3.4 (Nonlinear and Adaptive Control), Glasgow University has been active on WP 3.1 (Multivariable Control), the Hamilton Institute has contributed to WP 3.1, while Lund University has worked on WP 3.1, 3.2.

Contents

1 Introduction

In this final report on WP3 Controller Design, we present a consolidated framework of design methods as they are used in the relevant application work packages.

Workpackage 3 focuses on theoretical advances in control methods with the aim of applying these to the application work packages, *Vehicle control for active safety* (WP 1) and *Integrated Chassis control / Generic prototype* (WP 2). It was identified that the complex nonlinear control problems of these two work packages would require the combination of the advantages of a number of different control approaches, including classical multivariable control analysis and design (WP 3.1), hybrid control (WP 3.2), multivariable control with time delay (WP 3.3) and nonlinear and adaptive control (WP 3.4). While these topics represent a framework of design methodologies, the methods which we focused on were ultimately driven by the requirements evolving from the applications.

To ensure that our theoretical control developments are relevant to the application work packages of the project, each partner integrated their activities in WP 3 closely with the corresponding application work package. This is reflected in the structure of this report, where we present the control design methods as they related to the relevant application work package.

In sections 2 to 4 the control design framework for WP 1 *Vehicle control for active safety* is presented.

Section 2 focuses on the activities at Lund University with respect to *Roll-over protection* (WP 1.1). Methods relating to multi-variable control (WP 3.1) were used. As the roll-over problem represents a hybrid system, corresponding methodology had to be developed (WP 3.2), with a central aspect being handling of constraints and control allocation. Quadratic programming methods were adapted to solve the corresponding optimisation problems.

Section 3 describes the activities at Glasgow University relating to controller design for collision avoidance (WP 1.2). The work focused on aspects of multi-variable control (WP 3.1), applying this to the highly non-linear problem of controlling a vehicle during a collision avoidance manoeuvre.

In section 4, a dynamic control allocation algorithm for yaw stabilisation is presented which was developed at SINTEF. The method offers functionality similar to the Electronic Stability Program (ESP), using the brakes as actuators. The approach is modular and combines convergence and stability properties for yaw rate tracking, optimality of the allocation problem (WP 3.2) and adaptation of the maximal tyre-road friction parameter (WP 3.4). This activity is related to both applications of work package 1, where yaw stabilisation is an underlying control requirement.

The control design framework related to work package 2 (*Integrated Chassis control / Generic prototype*) is presented in section 5, describing the relevant activities at the Hamilton Institute. The approach focuses on multi-variable control design and analysis based on the ICD framework (WP 3.1).

2 Controller Design for Rollover Prevention (WP 1.1)

2.1 Introduction

Work Package 1.1 deals with the development of advanced controllers for vehicle rollover prevention. Although work has previously been done on this application, much of it deals with 'passive' systems such as rollover warning [1]. Among the work done on control design, the use of simple linear models is prevalent [2, 3], as is common for vehicle dynamics control. Although different actuator combinations have been investigated [4, 3], explicit handling of the complicated (and very important) constraints associated with the actuators (primarily the brakes) is often lacking.

The aim of the workpackage is to develop advanced controllers for the rollover prevention problem which are capable of operating during extreme driving conditions. In this report the control strategy will be described. To begin with, some practical considerations which help to define the problem will be mentioned. The overall control strategy will then be described. Finally, the details of the control design will be presented.

2.1.1 Practical Considerations

The essential function of the rollover controller is to prevent driver-induced (untripped) rollover accidents by means of various actuators. The system should be capable of preventing rollover for a range of loading conditions, and should not restrict vehicle performance more than necessary.

Actuators: Potential actuator choices include braking systems where brake pressures can be individually assigned, steer-by-wire systems and active suspension systems. Within the context of this project the primary interest is using the brakes as actuators. In Deliverable D11 an experimental vehicle intended for research in rollover prevention is described. This vehicle is equipped with electronic brake force distribution (EBD) which allows brake torques at each wheel to be individually assigned. In this way braking commands can be used to directly influence both the longitudinal velocity u and the yaw rate $\dot{\psi}$.

Available Inputs: It is assumed that the following vehicle states are available, either through measurement or estimation:

State	Description
u	Longitudinal velocity
v	Lateral velocity
$\dot{\psi}$	Yaw rate
$\dot{\phi}$	Roll rate
ϕ	Roll angle

Additional signals that are assumed to be available include:

Signal	Description
a_y	Lateral acceleration
δ	Steering angle
μ	Coefficient of friction
ω_i	Wheel angular velocities

$$\left(\frac{F_y}{F_{y,max}}\right)^2 + \left(\frac{F_x}{F_{x,max}}\right)^2 = 1$$
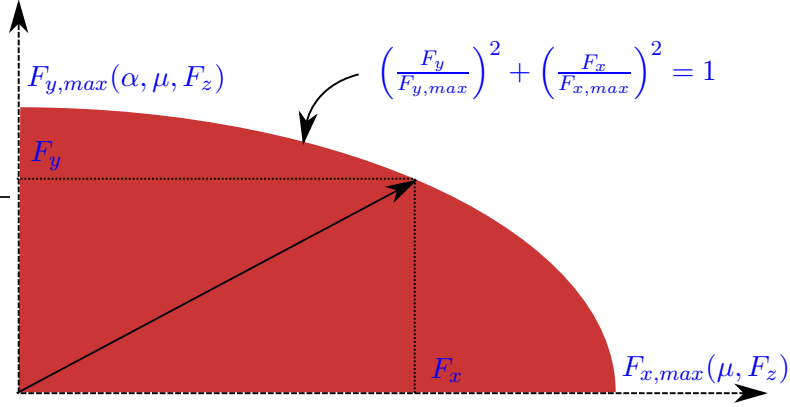
Figure 1: Illustration of the friction ellipse approximation of the tire force characteristics

Controller Outputs: Vehicle modelling is often performed by considering resultant forces and moments acting on the vehicle chassis (see Deliverable D1). These forces are derived from forces at each of the tires. Controllers based on such models will therefore have outputs expressed as forces. The inputs to the brake actuators are pressures, so a conversion between brake pressure and force at the tire contact point is required. This can be done with knowledge of the parameters of the brake actuators, the dynamic rolling radius of the tires, and an estimate of the road-tire friction coefficient.

Constraints: The rollover mitigation problem is characterised by a number of constraints, primarily involving the forces at the tire contact patch. These constraints are summarised by the so-called 'friction ellipse', illustrated in Figure 1. This implies that the resultant tire force must lie within an ellipse, defined by the maximum available lateral and longitudinal forces. The ellipse is described by the equation:

$$\left(\frac{F_y}{F_{y,max}}\right)^2 + \left(\frac{F_x}{F_{x,max}}\right)^2 = 1 \tag{1}$$

In fact, the resultant force is constrained to lie in one quadrant of the ellipse, since longitudinal forces must be negative (corresponding to braking), and the lateral force has a prescribed direction (determined by the sign of the tire slip angle α). The maximum longitudinal force is determined by the normal force F_z and the coefficient of friction μ. The maximum lateral force is given by the so-called 'Magic Formula' [5]. The reader is referred to Deliverable D1 or [6], [7] for further information on tire models.

Additional constraints arise from the actuators. The brakes have a number of performance constrains, outlined in Table 1.

Maximum pressure	200	bar
Time delay	10	msec
max. pressure build-up time 0-50 bar	200	msec
max. pressure build-up time 0-100 bar	500	msec
max. pressure reduction rate	-1000	bar/s

Table 1: Brake actuator constraints

2.2   Strategy

From the previous section it is obvious that a large number of constraints are present. In addition, the relationships between the actuators and the variables to be controlled are complex. This type of control problem is widely encountered in the vehicle control, in particular for aircraft and ships, where there are typically large numbers of actuators which affect the system dynamics in complex ways. In these cases it is typical to use the so-called *Control Allocation* approach, where the control design task is split into two parts. The control design is performed with respect to 'virtual controls' which are typically the generalized forces acting on the system. A control allocator is then used to map these virtual controls to actuator commands, while respecting the constraints. Figure 2 illustrates the structure of such control systems.

Using the control allocation structure, the actual control design problem becomes fairly simple. Controllers can be designed using the generalized forces and moments as inputs. The more difficult task of mapping these desired generalized forces to the actuator inputs, taking into account actuator constraints, is performed by the control allocator.

The rollover control strategy that has been implemented and successfully simulated has two control objectives:

- **Limitation of roll angle ϕ:** If the roll angle can be constrained with in a given interval of angles $|\phi| < \phi_{max}$, then vehicle rollover will not occur

- **Yaw rate tracking:** While roll control is being performed, the vehicle must simultaneously track a yaw rate reference $\dot{\psi}_{ref}$

Control of the vehicle sideslip angle β is also important, but this has not been implemented explicitly. Instead, it can seen experimentally that the sideslip angle is bounded when yaw rate control is performed.
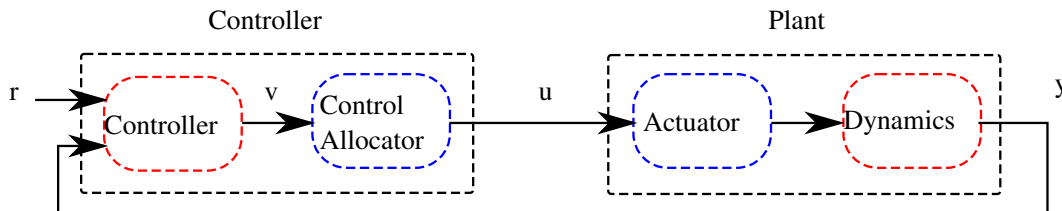

Figure 2: Control Allocation block diagram

The following sections describe in more detail the derivation of the control laws, the theory of control allocation, as well as the design of the control allocator.

2.3 Control Design

2.3.1 Chassis Model

In order to adequately describe the dynamics of the vehicle, a nonlinear two–track model with roll dynamics can be used. Figure 3 illustrates the model in the vertical plane. The suspension is modelled by a torsional spring–damper system, with roll stiffness C_ϕ and damping K_ϕ. The model is given by [5]:

$$
\begin{pmatrix}
m & 0 & -mh\phi & 0 & 0 \\
0 & m & 0 & mh & 0 \\
-mh\phi & 0 & I_z & I_z\theta_r - I_{xz} & 0 \\
0 & mh & I_z\theta_r - I_{xz} & I_x + mh^2 & K_\phi \\
0 & 0 & 0 & 0 & 1
\end{pmatrix}
\begin{pmatrix}
\dot{v_x} \\
\dot{v_y} \\
\ddot{\psi} \\
\ddot{\phi} \\
\dot{\phi}
\end{pmatrix}
\tag{2}
$$

$$
=
\begin{pmatrix}
F_{xT} + m\dot{\psi}v + 2mh\dot{\phi}\dot{\psi} \\
F_{yT} - m\dot{\psi}u + mh\dot{\psi}^2\phi \\
M_T - mhv\dot{\psi}\phi \\
-mhu\dot{\psi} + (mh^2 + I_y - I_z)\dot{\psi}^2\phi - (C_\phi - mgh)\phi \\
\dot{\phi}
\end{pmatrix}
$$

where the states are longitudinal velocity v_x, lateral velocity v_y, yaw rate $\dot{\psi}$, roll rate $\dot{\phi}$ and roll angle ϕ. The inputs to the system are the total longitudinal force F_{xT}, total lateral force F_{yT}, and total moment M_T. The relationship between the individual tire forces and these total forces will be derived in Section 2.4.5. The model parameters are described in Table 2. The model (2) is on differential algebraic equation (DAE) form, making it difficult to use for control design. If θ_r and the product of inertia I_{xz} are small, then the term $(I_z\theta_r - I_{xz})$ can be neglected (this corresponds to neglecting the direct couplings between the yaw and roll accelerations). The following ODE model may then be obtained:

$$
\begin{aligned}
\dot{v_x} =& \frac{I_z(F_{xT} + m\dot{\psi}v_y + 2mh\dot{\phi}\dot{\psi}) + m\phi h(M_T - mhv_y\dot{\psi}\phi)}{m(I_z + h^2\phi^2 m)} \\
\dot{v_y} =& \frac{(F_{yT} - m\dot{\psi}v_x + mh\phi\dot{\psi}^2)(I_x + mh^2)}{mI_x} \\
& + \frac{h(mh\dot{\psi}v_x + C_\phi\phi + K_\phi\dot{\phi} - (mh^2 + I_y - I_z)\dot{\psi}^2\phi)}{I_x} \\
\ddot{\psi} =& \frac{M_T + F_{xT}\phi h + 2mh^2\phi\dot{\phi}\dot{\psi}}{I_z - h^2\phi^2 m} \\
\ddot{\phi} =& \frac{-F_{yT}h - (C_\phi + (I_z - I_y)\dot{\psi}^2)\phi - K_\phi\dot{\phi}}{I_x}
\end{aligned}
\tag{3}
$$

The control task consists of two parts. Primarily, vehicle rollover must be prevented. Secondly, the yaw rate must be stabilized, and should track a reference. This

Mv^2/ρ

Mg

ϕ

h

$c_\phi\phi + k_\phi\dot{\phi}$

r_0

l

F_{yR} F_{zL} F_{yL} F_{zL}
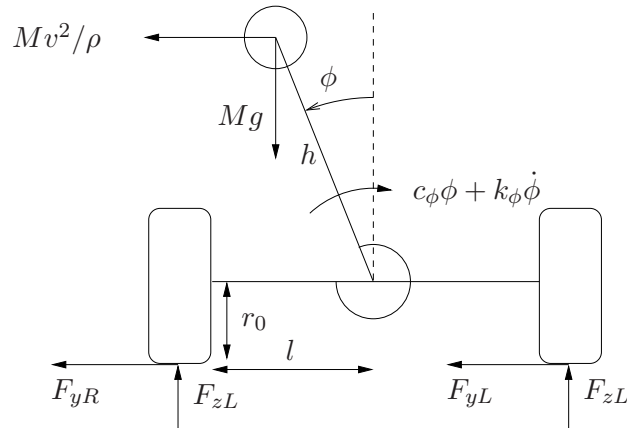
Figure 3: The two-track model in the vertical plane

Table 2: Parameters of the two–track model

Symbol	Description
m	Vehicle mass
h	Height of CoG above roll axis
I_x	Moment of inertia about x–axis
I_y	Moment of inertia about y–axis
I_z	Moment of inertia about z–axis
I_{xz}	Product of inertia for x and z axes
a	Distance from front axle to CoG position (along x–axis)
b	Distance from rear axle to CoG position (along x–axis)
l	Half track width
C_ϕ	Total roll stiffness
K_ϕ	Total roll damping
θ_r	Angle between roll axis and x–axis

ψ

y

ϕ

x

z

Figure 4: Vehicle diagram

secondary control objective is important, since the extreme maneuvering giving rise to a potential rollover may be necessary to avoid an obstacle, or remain on the road. Restriction of the vehicle sideslip angle β (the angle between the vehicle-fixed x-axis and the velocity vector) is also important, but this can be accomplished through appropriate yaw rate control [8].

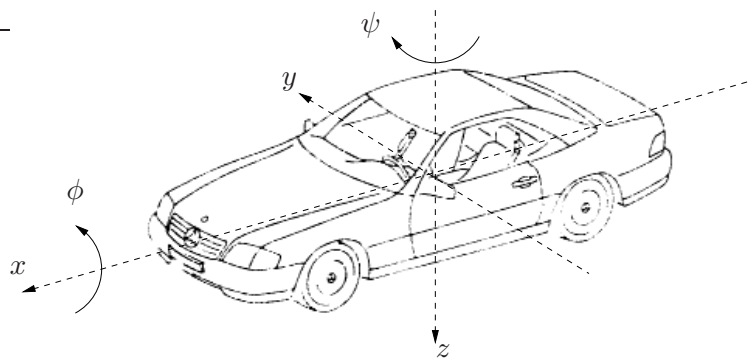For the design, the generalized forces and moments, or *virtual controls* $v = \begin{pmatrix} F_{xT} & F_{yT} & M_T \end{pmatrix}^T$ will be used. The task of obtaining the individual braking forces from given virtual controls is performed by the control allocator, described in the next section.

The strategy for roll control adopted here is to define a maximum allowable roll angle ϕ_{max} and design a controller to ensure that this limit is never exceeded. The choice of ϕ_{max} could come from an analysis of the dynamics of rollover, or could simply be chosen by experiment. Once a value of ϕ_{max} is decided, a corresponding limit on the total lateral force F_{yT} may be determined. From the friction ellipse, it can be seen that F_{yT} can be influenced by varying the total longitudinal (braking) force F_{xT}. The choice of F_{xT} constitutes the first part of the control design task. Yaw motion must then be controlled via the total moment M_T.

2.3.2 Roll Control

A bound on the roll angle may be translated into a bound on F_{yT} in the following way. From (3), the roll dynamics are described by:

$$I_x\ddot{\phi} + (C_\phi + (I_z - I_y)\dot{\psi}^2)\phi + K_\phi\dot{\phi} = - F_{yT}h$$

For practical values of the parameters and states, the term involving $\dot{\psi}$ is small enough to be neglected, resulting in linear SISO system, for which the transfer function from lateral force F_{yT} to roll angle ϕ is given by:

$$G_{roll}(s) = \frac{-h}{I_x s^2 + K_\phi s + C_\phi} \tag{4}$$

with corresponding impulse response $g_{roll}(t)$. The roll angle ϕ is given by:

$$\phi(t) = \int_0^\infty F_{yT}(t - \tau)g_{roll}(\tau)d\tau \tag{5}$$

$$\leq ||F_{yT}|| \underbrace{\int_0^\infty |g_{roll}(\tau)|d\tau}_{||G_{roll}||_{L_1}} \tag{6}$$

If the maximum allowable roll angle is given by ϕ_{max}, then the following inequality is obtained:

$$||F_{yT}|| \leq \frac{\phi_{max}}{||G_{roll}||_{L_1}} \tag{7}$$

Recalling the idea of the friction ellipse, it is possible to limit F_{yT} by choosing F_{xT} sufficiently large. By considering a friction ellipse for the entire vehicle, the

following approximate relation is obtained:

$$F_{xT} \approx F_{xT,max} \sqrt{1 - \left(\frac{F_{yT}}{F_{yT,max}}\right)^2} \qquad (8)$$

where $F_{xT,max}$ and $F_{yT,max}$ are the maximum attainable generalized forces. Substituting the condition (7) into (8) gives:

$$|F_{xT}| \geq F_{xT,max} \sqrt{1 - \left(\frac{\phi_{max}}{F_{yT,max}||G_{roll}||_{L_1}}\right)^2} \qquad (9)$$

A proportional controller may now be dimensioned using (9) such that the maximum allowable lateral force is never exceeded. It should be noted that some tuning may be required if the bound (7) is too conservative. Although it is not possible to measure F_{yT} directly, the lateral acceleration a_y is normally measured in vehicles equipped with ESP systems. Thus the relation $F_{yT} = ma_y$ may be used. The total longitudinal force F_{xT} is regarded as the virtual control signal, and the control law is given by:

$$F_{xT} = -K_x m |a_y| \qquad (10)$$

The gain K_x can be chosen so that the maximum allowable lateral force results in a control action satisfying (9). The switching of the controller is related to the problem of detection (or prediction) of an imminent rollover event, which is not studied in depth here. Rollover detection is treated in [9] and [10]. A simple switching strategy involves determining a threshold value of a_y and using this as a switching condition. A smoothing function is required to provide smooth transitions between on and off modes. The control law then becomes:

$$F_{xT} = \begin{cases} -K_x \Upsilon m |a_y| & |a_y| \geq a_{y,threshold} \\ 0 & |a_y| < a_{y,threshold} \end{cases} \qquad (11)$$

where Υ is a suitable smoothing function.

2.3.3 Yaw Control

Attention may now be directed at controlling the yaw rate $\dot{\psi}$. From (3), it can be seen that the yaw rate can be influenced by both M_T and F_{xT}. A simple Lyapunov function for the yaw dynamics is given by:

$$V_r(x, v) = \frac{1}{2}(\dot{\psi} - \dot{\psi}_{ref})^2 \qquad (12)$$

with derivative:

$$\frac{dV(x, v)}{dt} = \frac{\partial V_r(x, v)}{\partial \dot{\psi}} \frac{\partial \dot{\psi}}{\partial t} = (\dot{\psi} - \dot{\psi}_{ref})\ddot{\psi} \qquad (13)$$

By choosing F_{xT} and M_T such that $\ddot{\psi} = -K_r(\dot{\psi} - \dot{\psi}_{ref})$, the Lyapunov derivative becomes:

$$\frac{dV(x,v)}{dt} = -K_r(\dot{\psi} - \dot{\psi}_{ref})^2 \tag{14}$$

rendering the equilibrium $\dot{\psi} = \dot{\psi}_{ref}$ globally asymptotically stable. Since F_{xT} is given by (11), M_T may be obtained from:

$$M_T = -K_r(\dot{\psi} - \dot{\psi}_{ref})(I_z - h^2\phi^2 m) - 2mh^2\phi\dot{\phi}\dot{\psi} \tag{15}$$
$$-h\phi F_{xT}$$

2.4 Control Allocation

2.4.1 Background

In traditional control design, the control signal is assumed to be the actual input to the system. This input could be a valve position, a voltage or current, or any number of other physical quantities. Although this assumption is reasonable in most cases, there exist control design tasks which are less well suited to this approach. This is particularly true in the case of vehicle control. Road vehicles, aircraft and ships typically have large number of actuators, which often affect the vehicles' dynamics in complex ways. Aircraft have many control surfaces which can be used in different ways to produce movement.

A key issue is redundancy: the same control action can be produced in many different ways using different combinations of the actuators. It is clear that the 'control action' being referred to here is some abstract quantity. Because of this it is attractive to perform control design based on control signals which are not the same as the actual inputs to the system. For model-based control design, it is often easier to work with models describing the response of the system to external forces and moments, rather than actuator positions or voltages. In the aircraft example, the dynamic model of the system uses resultant forces and moments acting on the aircraft, rather than actuator positions. In vehicle control for instance it is very common to use resultant forces and moments acting on the vehicle as control signals, rather than actuator positions. The control design task is effectively spilt into two parts. In the first part, standard control design methods are used to obtain 'virtual' control signals. The second part consists of transforming these virtual control signals into actual control signals which may be applied to the process to be controlled.

Although the mapping between actuator inputs and generalized forces and moments may usually be considered static, there are a number of good reasons for not using the actual control signals directly.

Control allocation is typically used for over-actuated systems, in which there are more actuator inputs than 'virtual' control inputs. Returning to the aircraft example, the virtual controls or generalized forces consist of three forces and three moments. However, depending on the aircraft configuration, there may be a large number of different actuators which may be used to obtain these resultant forces and moments. These could include elevators, ailerons, canard foreplanes, thrust
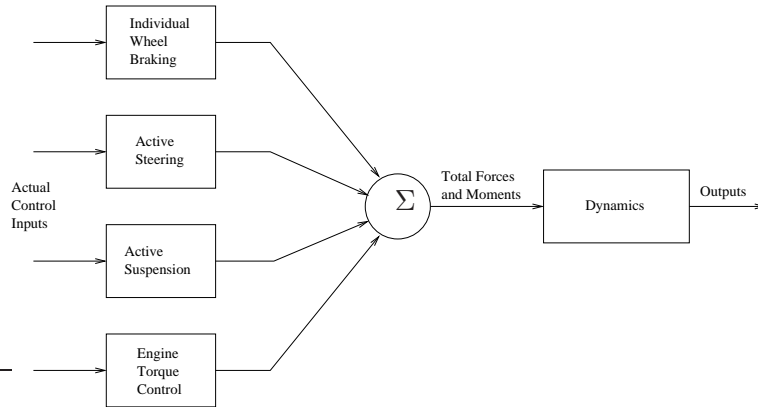
Figure 5: Block diagram illustrating the separation of actuator contributions and vehicle dynamics

vectoring and more. Similarly, for a road vehicle, resultant forces and moments may be achieved by using individual wheel braking, active steering, and active suspension.

As a simple example, consider a system with m actuators:

$$\dot{x} = Ax + Bu$$

where $u = \sum_{i=1}^{m} u_i$ is the resultant control signal and u_i are the contributions of the individual actuators. Control synthesis yields a stabilizing control law u_v. There are many choices of actuator inputs that yield $u_v = \sum_{i=1}^{m} u_i$, and it is the task of the control allocator to find the 'best' combination in some sense.

An additional complication arises when constraints are imposed on the actuators, as is practically always the case in applications. In this case the control allocator must choose a combination of actuator inputs which give the desired result while satisfying the constraints.

2.4.2 Problem Formulation

The role of the control allocator is to obtain *actual controls* which will give rise to the desired *virtual controls*. In general, the relationship is $v(t) = g(u(t))$ where $v(t) \in \mathbb{R}^k$ are the virtual controls, $u(t) \in \mathbb{R}^m$ are the actual controls and $g : \mathbb{R}^m \to \mathbb{R}^k$ is the mapping from actual to virtual controls, where $m > k$. The majority of the literature deals with the linear case [11], where the actual and virtual controls are related by a *control effectiveness matrix* B:

$$v(t) = Bu(t) \tag{16}$$

The control allocation problem is an under-determined, and often constrained problem. A wide variety of methods exist for solving allocation problems, many of which are reviewed in [11]. A common approach is to formulate an optimization problem in which the magnitude of the allocation error:

$$\epsilon = ||Bu(t) - v(t)||_p, \quad p = 1, 2, \ldots$$

is minimized, subject to constraints and possibly additional costs on actuator use. The choice of norm will be discussed later.

An important requirement imposed on the control allocation algorithm is that it must be implementable in a real-time environment. This is particularly important in automotive contexts, where sample times are typically of the order of 10ms. Algorithms with high levels of computational complexity are therefore not well suited to the application. Another requirement, particularly relevant to automotive applications, is that the number of sensors must be kept to a minimum. It is therefore desirable to use the minimum possible number of signals in control design.

2.4.3 Convex Optimization

In order to use optimization for control allocation, it is natural to construct convex optimization problems. Such problems posses many attractive properties, and efficient solvers exist for a wide range of problem formulations. Additionally, a very large number of problems can be posed as convex optimization problems. In this section, a number of different problem formulations will be outlined. In the following section, methods for solving these types of problems will be reviewed.

The general form of a convex optimization problem is:

$$
\begin{aligned}
&\text{minimize} && f_0(x) \\
&\text{subject to} && f_i(x) \le b_i, && i = 1, \ldots, m
\end{aligned}
$$

in which the objective function $f_0(x)$ and the constraints $f_i(x) \le b_i$ are convex functions. The *feasible set* $\mathcal{P}$ of the optimization problem is the region in which the constraints are satisfied. The optimum x^* is the point in the feasible set where the objective function (also called cost function) is minimized. A number of sub–classes of convex problems exists, a number of which are outlined below.

Linear Programs: Linear Programs (LP) are convex problems in which both the objective and constraint functions are affine. They have the form:

$$
\begin{aligned}
&\text{minimize} && c^T x + d \\
&\text{subject to} && Gx \le h \\
&&& Ax = b
\end{aligned}
$$

The feasible set of an LP is a polyhedron, and since the objective function is linear, the level curves are given by hyperplanes orthogonal to c. The feasible set and level curves of a general LP are illustrated in Figure 6.

Quadratic Programs with Linear Constraints: In Quadratic Programs (QP), the objective function is convex quadratic. When linear constraints are present, the problem has the form:

$$
\begin{aligned}
&\text{minimize} && \frac{1}{2} x^T P x + q^T x + r \\
&\text{subject to} && Gx \le h \\
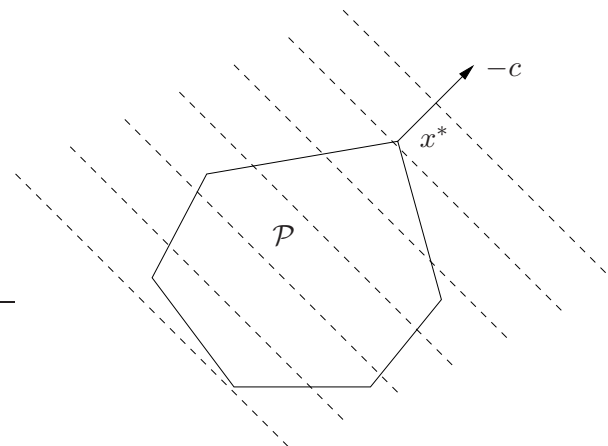&&& Ax = b
\end{aligned}
$$

Figure 6: Interpretation of the solution of an LP problem, showing the active set $\mathcal{P}$ and the level curves of the objective function, which are hyperplanes orthogonal to c
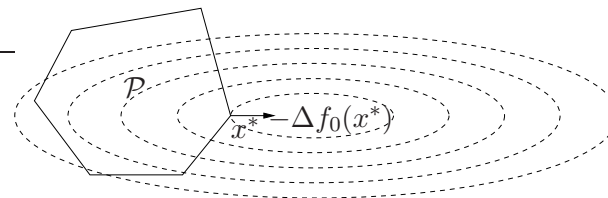

Figure 7: Interpretation of the solution of an QP problem, showing the active set $\mathcal{P}$ and the level curves of the objective function.

Figure 7 gives a graphical interpretation of a QP problem.

Quadratic Programs with Quadratic Constraints: Another class of QPs are those in which the both the objective function and the constraints are convex quadratic:

$$
\begin{aligned}
\text{minimize} \quad & \frac{1}{2}x^T P_0 x + q_0^T x + r_0 \\
\text{subject to} \quad & \frac{1}{2}x^T P_i x + q_i^T x + r_i \leq 0, \quad i = 1, \ldots, m \\
& Ax = b
\end{aligned}
$$

2.4.4 Solving Convex Optimization Problems

Posing control allocation problems as convex optimization problems is attractive since there are a wide variety of efficient solvers for different types of problems. One class of methods known as *Active Set* methods is particularly suitable, for several reasons. Primarily, active set algorithms have the appealing property that a feasible solution is available after each iteration. For applications in a real-time environment this is particularly useful, since it means that if the algorithm must be interrupted, a feasible (albeit suboptimal) solution will always be available. In addition, active
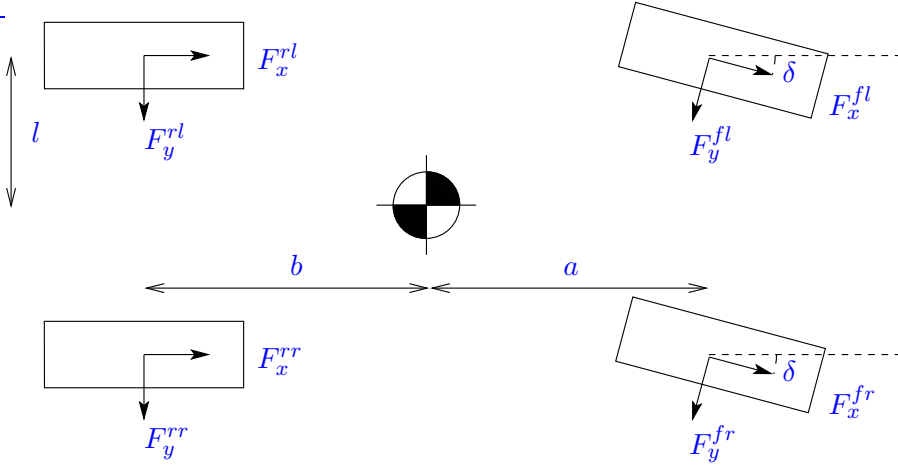
Figure 8: Planar chassis diagram showing the individual tire forces

set methods become much more efficient when a good estimate of the active set is available. For control allocation purposes, a good estimate of the active set is usually given by the active set from the previous sample. In order to maximize efficiency, the structure of the problem must be utilized to select the most effective solver. Active set methods for control allocation are discussed in more detail in [11].

2.4.5 Control Allocator Design

In this section two methods of performing control allocation for the rollover prevention problem will be proposed.

The control laws derived in the control design section use the generalized forces F_{xT}, F_{yT} and M_T as virtual controls. The aim of the control allocator is to obtain actual control signals which give rise to the desired virtual controls, while respecting certain constraints. The actual control signals in this case are taken to be the longitudinal tire forces. In reality the control commands are the brake pressures, but a simple relationship exists between these quantities.

Control Effectiveness Matrix Derivation: To begin with, regard both the longitudinal and lateral tire forces F_{xi} and F_{yi} are regarded as actual controls, with:

$$u_a = \begin{pmatrix} F_x^{fl} & F_x^{fr} & F_x^{rl} & F_x^{rr} & F_y^{fl} & F_y^{fr} & F_y^{rl} & F_y^{rr} \end{pmatrix}^T$$

where the superscripts on the individual forces denote the axle (front or rear) and side (left or right) of the wheel in question. Define the vector of virtual controls as:

$$u_v = \begin{pmatrix} F_{xT} \\ F_{yT} \\ M_T \end{pmatrix} \tag{17}$$

By considering Figure 8, the following expressions relating the individual tire forces

to the generalized forces are obtained:

$$F_{xT} = F_x^{rl} + F_x^{rr} + (F_x^{fl} + F_x^{fr})\cos\delta - (F_y^{fl} + F_y^{fr})\sin\delta \tag{18}$$

$$F_{yT} = F_y^{rl} + F_y^{rr} + (F_y^{fl} + F_y^{fr})\cos\delta + (F_x^{fl} + F_x^{fr})\sin\delta \tag{19}$$

$$M_T = (F_y^{fl} + F_y^{fr})a\cos\delta - (F_y^{rl} + F_y^{rr})b + (F_x^{fl} + F_x^{fr})a\sin\delta + \tag{20}$$

$$(F_x^{rl} + F_x^{fl}\cos\delta + F_y^{fr}\sin\delta - F_x^{rr} - F_x^{fr}\cos\delta - F_y^{fl}\sin\delta)l \tag{21}$$

where δ is the steering angle. The control effectiveness matrix is given by:

$$B^T = \begin{pmatrix} \cos\delta & \sin\delta & (a\sin\delta + l\cos\delta) \\ \cos\delta & \sin\delta & (a\sin\delta - l\cos\delta) \\ 1 & 0 & l \\ 1 & 0 & -l \\ -\sin\delta & \cos\delta & (a\cos\delta - l\sin\delta) \\ -\sin\delta & \cos\delta & (a\cos\delta + l\sin\delta) \\ 0 & 1 & -b \\ 0 & 1 & -b \end{pmatrix} \tag{22}$$

Method 1: Formulation of a QCQP Allocation Problem: For the rollover prevention problem, allocation based on convex optimization has been studied in [9].

From the equations relating individual tire forces to the virtual controls, the condition that must be satisfied for the virtual controls to be obtained is:

$$Bu_c = u_v \tag{23}$$

where:

A number of additional constraints are present. The control signals are purely braking forces (not tractive forces), giving rise to the constraint:

$$F_{xi} \leq 0 \tag{24}$$

The maximum allowable braking force is determined by the coefficient of friction μ between the tire and the road, as well as the vertical wheel load F_z, which can be expressed as:

$$F_{xi} \geq -|\mu F_{zi}| \tag{25}$$

The lateral force must act in the correct direction (the same direction as the maximum force F_{yiMax}). This can be expressed as:

$$F_{yi}F_{yiMax} \geq 0 \tag{26}$$

Finally, there are the constraints arising from the friction ellipse:

$$\left(\frac{F_y}{F_{y,max}}\right)^2 + \left(\frac{F_x}{F_{x,max}}\right)^2 \leq 1 \tag{27}$$

These constraints can be expressed as norm constraints, on the form:

$$||W_i u_c|| \leq 1 \tag{28}$$

where the matrices W_i have the form:

$$
W_{FL} = \begin{pmatrix}
\frac{1}{F_{yFL,max}} & 0 & 0 & 0 & 0 & 0 & 0 & 0 \\
0 & 0 & 0 & 0 & 0 & 0 & 0 & 0 \\
0 & 0 & 0 & 0 & 0 & 0 & 0 & 0 \\
0 & 0 & 0 & 0 & 0 & 0 & 0 & 0 \\
0 & 0 & 0 & 0 & \frac{1}{\mu F_{zFL}} & 0 & 0 & 0 \\
0 & 0 & 0 & 0 & 0 & 0 & 0 & 0 \\
0 & 0 & 0 & 0 & 0 & 0 & 0 & 0 \\
0 & 0 & 0 & 0 & 0 & 0 & 0 & 0
\end{pmatrix}
\tag{29}
$$

If a convex optimization problem is posed using the equality constraint (23), the presence of the other constraints may make the problem infeasible (no solution exists which satisfies all the constraints). To avoid this, a slack variable γ is introduced, and a second-order cone problem (SOCP) can be posed.

Replace the equality constraint (23) with the inequality:

$$
||Au_c - u_v|| \leq \gamma \tag{30}
$$

The optimization problem can be written as:

$$
\begin{align}
\text{minimize} \quad & \gamma \tag{31} \\
\text{subject to} \quad & ||Au_c - u_v|| \leq \gamma \tag{32} \\
& ||W_i u_c|| \leq 1 \tag{33} \\
& F_{yi} F_{yiMax} \geq 0 \tag{34} \\
& F_{xi} \leq 0 \tag{35} \\
& F_{xi} \geq -|\mu F_{zi}| \tag{36}
\end{align}
$$

The constraints arising from the friction ellipse are expressed as weighted-norm constraints and a quadratically-constrained quadratic program (QCQP) is formulated: This optimization problem must be solved in each sampling period, making this approach somewhat computationally expensive.

Method 2: Formulation of a LCQP Allocation Problem:

It is clear that some simplification of the problem may be advantageous. Regarding the computational complexity of the algorithm, a key issue is the type of constraints present. The constraints derived from the friction ellipse are quadratic, so algorithms capable of solving quadratically constrained problems would be required if these constraints were included in an optimization problem. In addition, the sideslip angles of the wheels α_i and the normal tire forces F_{zi} must be known in order to calculate the values of $F_{yi,max}$. This represents additional information which must be either measured or estimated. It is therefore proposed to make approximations which both simplify the constraints and reduce the amount of extra information required. Since the controller will be operating exclusively in the limits of the vehicle's driving regime, it is reasonable to make approximations which are valid during these conditions. The first approximation is that the slip angles of all of the wheels are large enough such that the maximum lateral tire forces saturate,
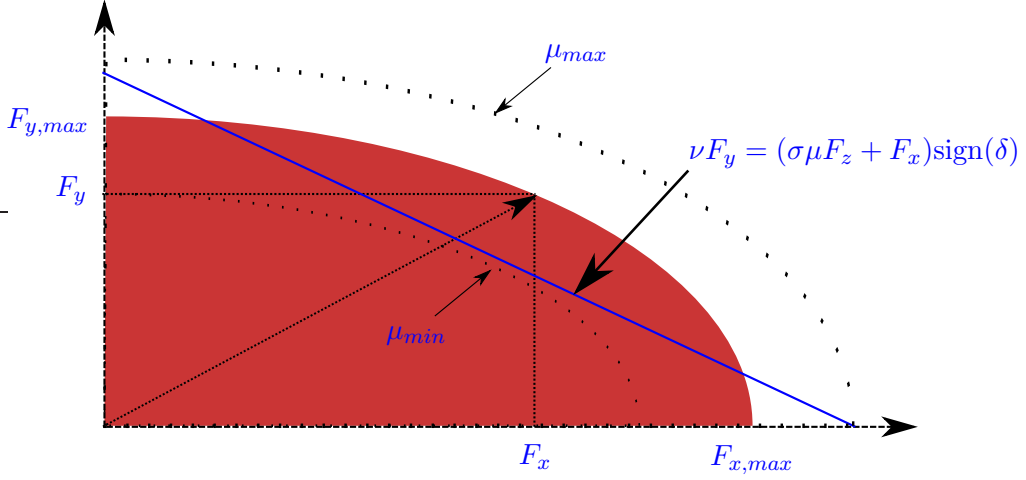
Figure 9: The friction ellipse with linear approximation, showing the uncertainty regions arising from the uncertainty of μ

and are thus given by $F_{yi,max} = \mu F_{zi}$. This is attractive since the slip angles are no longer required in order to compute the maximum lateral forces. The resultant force on each wheel can now be seen as a function of the applied braking force and the normal force. However, the function is still nonlinear (the friction ellipse becomes a circle when $F_{yi,max} = F_{xi,max}$), so a further approximation is suggested to simplify the constraints. The friction circle can be approximated in each quadrant by a linear function, as in Figure 9. This approximation can be justified by considering that there will be a large amount of uncertainty in the radius of the friction circle. In particular, μ is highly uncertain. The linear approximation can be thought of as lying within circles defined by upper and lower bounds of the radius μF_z. The approximation may be refined by introducing tuning parameters to alter the gradient and position of the linear approximations, giving a relationship on the form:

$$\nu F_y = (\sigma \mu F_z + F_x)\mathrm{sign}(\delta) \tag{37}$$

where $\nu, \sigma > 0$ are tuning parameters. The $\mathrm{sign}(\delta)$ factor is required to ensure that the resultant force acts in the correct direction. This approximation has the attractive property that the constraints are convex. In the formulation (31), it is assumed that the resultant force lies within the ellipse, rather than on the boundary, in order to obtain convex constraints. Using these simplifications, a new control allocation problem can now be formulated.

Replacing F_y with the linear approximation (37), the relationships can be written as:

$$F_{xT} = G_1 u + b_1 \tag{38}$$
$$F_{yT} = G_2 u + b_2 \tag{39}$$
$$M_T = G_3 u + b_3 \tag{40}$$

with $u = \begin{pmatrix} F_x^{fl} & F_x^{fr} & F_x^{rl} & F_x^{rr} \end{pmatrix}^T$. The matrices G_i and the vectors b_i depend on the normal forces F_{zi}. This gives the desired linear relationship between actual and

virtual controls:

$$v(t) = Gu(t) + b \qquad (41)$$

The constraints are now given by:

$$-|\mu F_{zi}| \leq F_{xi} \leq 0 \qquad (42)$$

A linearly-constrained quadratic programming problem may now be formulated. Such problems can take the form:

$$u = \arg\min_{u \in \Omega} ||W_u(u - u_d)||_2$$
$$\Omega = \arg\min_{\underline{u} \leq u \leq \overline{u}} ||W_v(Bu - v)||_2 \qquad (43)$$

where W_u and W_u are diagonal weighting matrices, u_d is a desired actual control value, and u_{min} and u_{max} are constraints on the actual controls. This type of problem is known as Sequential Least-Squares (SLS), since the solution is computed in two steps. First, the weighted allocation error $||W_v(Bu-v)||$ is minimized. If feasible solutions are found, then the 'best' solution is obtained by minimizing $||W_u(u-u_d)||$. This class of problems may be efficiently solved by active set methods [11]. An advantage of such methods is that feasible solutions are available after each iteration, meaning that the algorithm can be interrupted, yet still give a feasible (although suboptimal) solution. A faster algorithm can be obtained by approximating the SLS formulation as a Weighted Least-Squares (WLS) problem:

$$u = \arg\min_{\underline{u} \leq u \leq \overline{u}} \left(||W_u(u - u_d)||_2^2 + \gamma ||W_v(Bu - v)||_2^2 \right) \qquad (44)$$

Here, the solution is calculated in a single step. The parameter γ is typically chosen to be very large in order to emphasize the importance of minimizing the allocation error. This type of problem may be solved much faster than the QCQP problem described earlier and is therefore more suited to real-time applications. In the results presented here, the WLS algorithm (44) has been used.

Since only F_{xT} and M_T are used as virtual controls, F_{yT} may effectively be removed from the allocation problem by making the corresponding weight in the matrix W_v very small.

3 Controller Design for Collision Avoidance (WP 1.2)

3.1 Introduction

This section of the report presents aspects of control design useful for emergency lateral collision avoidance. The work has been undertaken in support of work package 1.2. Parts of the design methods described here can be found in [12].

The controller requirements are specified in interim report D7. The controller is required to cause a passenger vehicle to perform an aggressive lateral manoeuvre, navigating through a cone-bounded obstacle at high speed. The obstacle course is derived from ISO 3888 [13, 14] which specifies test track layouts for two severe lane-change manoeuvres. Part 1 describes a layout for a double lane-change while Part 2 describes a layout for obstacle avoidance. The manoeuvres are similar to each other but the obstacle avoidance track requires greater lateral movement of the vehicle to be accomplished within a more tightly constrained space; it is thus the more challenging of the manoeuvres and has been selected as the basis for the primary objective of this work.

However, the manoeuvres specified in ISO 3888 are designed primarily for testing the handling qualities of a vehicle. For an active safety system with no knowledge of the road ahead of the obstacle, it is more sensible for control of the vehicle to be returned to the driver as soon as the immediate danger has passed rather than attempting to return to the original lane. Furthermore, in an emergency situation, it is often wise to reduce the vehicle speed to increase the probability of avoiding an accident and to mitigate the effects of any crash that may occur; but it would be dangerous to overtake an obstacle - that might be moving - and to then slow down in front of it. Thus it is appropriate to use only the first part of the specified manoeuvre; the initial single-lane change.

Following the recommendations within the standard, the manoeuvre will be tested at a speed of 80 [km/hr]. Safety considerations would prevent much higher speeds from being attempted at the track where the controller will ultimately be tested on a real vehicle.

Section	Length	Lane offset	Width
1	15	-	$1.1 \times$ vehicle width + 0.25
2	30	-	
3	25	3.5	$1.2 \times$ vehicle width + 0.25
4	25	-	
5	15	-	$1.3 \times$ vehicle width + 0.25
6	15	-	$1.3 \times$ vehicle width + 0.25

Table 3: Dimensions of the double lane-change track (figure 10)

The vehicle dynamics are complex and highly non-linear. Furthermore, to achieve tracking of a target trajectory while maintaining directional stability, it is necessary to simultaneously control multiple actuators in response to measurements from multiple sensors. The system is therefore multi-input, multi-output (MIMO).
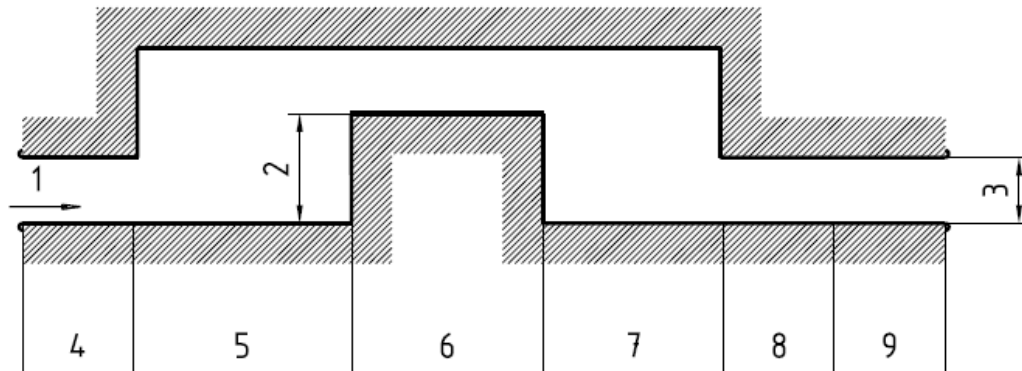
Figure 10: Double lane change (ISO 3888-1 [13])

Key:

1	*Driving direction*	*4*	*Section 1*	*7*	*Section 4*
2	*Lane offset*	*5*	*Section 2*	*8*	*Section 5*
3	*Width*	*6*	*Section 3*	*9*	*Section 6*

The dimensions of each section are specified in table 3
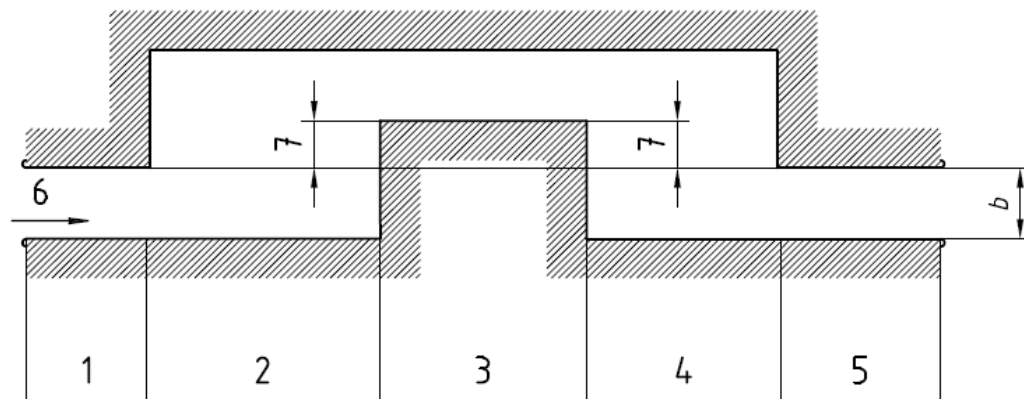
Figure 11: Obstacle avoidance (ISO 3888-2 [14])

Key:

1	*Section 1*	*4*	*Section 4*	*7*	*Lane offset*
2	*Section 2*	*5*	*Section 5*		
3	*Section 3*	*6*	*Driving direction*		

The dimensions of each section are specified in table 4

Section	Length	Lane offset	Width b
1	12	-	$1.1 \times$ vehicle width + 0.25
2	13.5	-	-
3	11	1	1.2 vehicle width + 1
4^a	12.5	-	-
5	12	-	$1.3 \times$ vehicle width + 0.25m but not less than 3 m
^{a} To ensure high accelerations at the end of the track, section 4 is 1 m shorter than section 2.

Table 4: Dimensions of the obstacle avoidance track (figure 11)

Five control inputs are available; the front wheel steering angle (δ) and independent longitudinal brake forces (f_x) on each of the four wheels. The vehicle is equipped with numerous sensors including accelerometers, tachometers and a global positioning sensor. Moreover, an observer developed in work package 4 allows best estimates of applicable system states to be provided in a timely manner.

3.2 Control architecture overview

The overall controller architecture is shown in figure 12. Significant features of the design are the use of feedforward control, obtained using inversion of static linear models, proportional feedback control and control allocation among redundant actuators by inverting part of a linearisation of a nonlinear dynamic model.
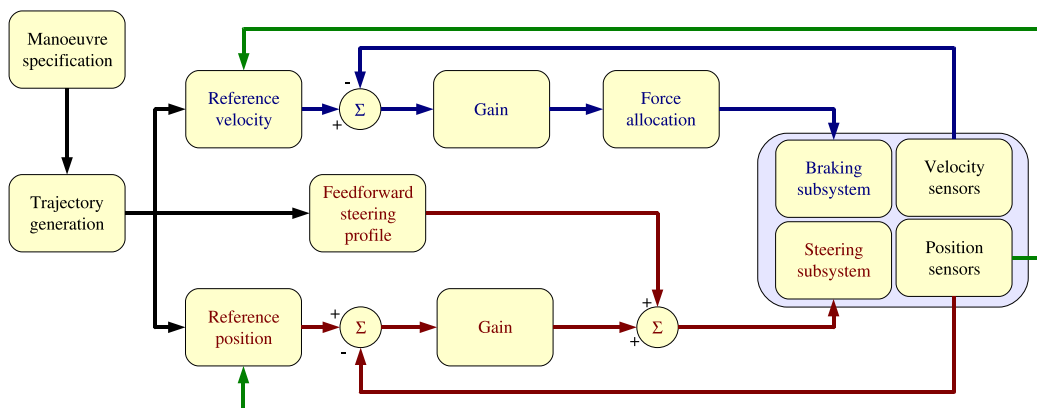
Figure 12: Controller architecture

At initialisation, a feasible trajectory is identified to enable the vehicle to complete the specified manoeuvre while remaining within its performance envelope. Reference profiles for the vehicle position and velocity are calculated for the entire manoeuvre, along with a nominal steering profile. As the manoeuvre progresses, proportional feedback control corrects for errors in the vehicle position and velocity using the steering and braking actuators.

An initialisation of the controller prior to execution of the manoeuvre generates

static look-up tables which are used to provide nominal feedforward control inputs and reference outputs throughout execution of the manoeuvre. Pre-processed look-up tables were chosen instead of real time calculation of reference signals because they are computationally efficient and can be guaranteed to provide a value within a specified time, thus making them suitable for a real time embedded system provided that there is sufficient memory available.

3.2.1   Initialisation

The first stage in the initialisation process is the identification of a feasible trajectory given the spacial limits of the track layout and the performance limits of the vehicle. Reference profiles for three vehicle states are then calculated: lateral position ($Y_{\oplus}^{*}$), yaw angle ($\Psi_{\oplus}^{*}$) and yaw rate ($\dot{\Psi}_{\oplus}^{*}$). These reference profiles are used to calcualate a nominal steering angle (δ_0) profile which will be used as a feedforward control signal during execution of the manouevre. A further brake force (f_x) profile can also be generated to cause the vehicle to decelerate on its approach to the first turn. Look-up tables are implemented using these five profiles, with longitudinal position ($X_{\oplus}$) as the independent variable.

3.2.2   Execution

During execution of the manoeuvre, feedback controllers are used to keep the vehicle following the specified reference profiles. These controllers are required to account for unmodelled dynamics in the feedforward controllers, parameteric uncertainties, and external disturbances. Augmentation of the steering angle is used to correct errors in position and braking is used to correct velocity errors.

3.3   Manoeuvre specification

The first step in determining the control inputs is the identification of a feasible path $Y_{\oplus}^{*}(X_{\oplus})$ for the vehicle to follow. A number of assumptions are made at this stage, but it should be noted that these assumptions may be further refined as work continues in work package 1.2 and results from tests on real hardware highlight changes required for the controller.

It is assumed that the vehicle will execute the manoeuvre at a constant forward speed. This assumption will certainly be violated during agressive manoeuvres when significant brake forces will slow the vehicle considerably. It is also assumed that the friction coefficient μ between the road and the tyres will be known and constant throughout the test. For the purposes of testing the controller, it is further assumed that this value is close to unity, as would be the case when using good tyres on dry asphalt. Finally it is assumed that the vehicle possesses no means of propulsion that does not act through the tyres, such as aerodynamic control surfaces.

Under these assumptions, the maximum acceleration that the vehicle is capable of performing will be $a_{max} = \mu\, g$ [m/s] in any direction where g is the constant of gravitational acceleration (≈ 9.81 [m/s^2]). Directing this acceleration vector to the side of the car would cause it to turn in the smallest possible circle that is achievable

without braking. The radius of this circle is $r = \frac{\dot{x}^2}{a_{max}}$ [m] where $\dot{x}$ is the forward speed of the vehicle.

An aggressive but feasible manoeuvre can therefore be identified by finding circles of radius r that will cause the vehicle to avoid the boundaries of the track and joining arcs of these circles with mutual tangents.

For the obstacle avoidance track layout, this method will work for speeds slightly in excess of 80 [km/hr], the speed at which the test is to be performed. For higher speeds it would be necessary to rely on braking during the turn to slow the vehicle and thus allow it to turn more sharply.

3.4 Trajectory generation

Given a specified path $Y_\oplus^*(X_\oplus)$ relative to the Earth that the vehicle is required to track, and assuming that the vehicle should always be oriented tangentially to the path that is being followed, it is possible to determine the required yaw angle $\Psi_\oplus^*$ and rate $\dot{\Psi}_\oplus^*$ at each point along the trajectory.

The requirement for tangential orientation is satisfied by requiring the reference yaw rate to be defined as a function of the path gradient: $\Psi_\oplus^* = \arctan \frac{\mathrm{d}Y_\oplus^*}{\mathrm{d}X_\oplus}$. Calculating the longitudinal velocity of the vehicle, relative to the Earth, as $\dot{X}_\oplus = \dot{x} \cos \Psi_\oplus - \dot{y} \sin \Psi_\oplus$ where $\dot{x}$ and $\dot{y}$ are the forward and lateral speed of the vehicle in its own body axis system, the reference lateral velocity and yaw rate (relative to the Earth) are given by

$$\dot{Y}_\oplus^* = \dot{X}_\oplus \frac{\mathrm{d}Y_\oplus^*}{\mathrm{d}X_\oplus} \tag{45}$$

$$\dot{\Psi}_\oplus^* = \dot{X}_\oplus \frac{\mathrm{d}\Psi_\oplus^*}{\mathrm{d}X_\oplus} \tag{46}$$

Rotation of the axis system by the vehicle yaw angle then yields the reference body velocities $(\dot{x}, \dot{y}, \dot{\psi})$ that the vehicle should track

$$\begin{pmatrix} \dot{x}^* \\ \dot{y}^* \\ \dot{\psi}^* \end{pmatrix} = \begin{pmatrix} +\cos \Psi_\oplus & +\sin \Psi_\oplus & 0 \\ -\sin \Psi_\oplus & +\cos \Psi_\oplus & 0 \\ 0 & 0 & 1 \end{pmatrix} \begin{pmatrix} \dot{X}_\oplus \\ \dot{Y}_\oplus^* \\ \dot{\Psi}_\oplus^* \end{pmatrix}$$

3.5 Steer-by-wire

There are two components to the steering control. A nominal feedforward signal δ_0 is augmented by a proportional feedback position controller.

3.5.1 Feedforward steering angle

The use of a feedforward controller enables the most significant element of the control signal to be independent of a measured error signal. Consequently, other parts of the controller need not be as sensitive as would otherwise be the case, thus enhancing system stability.

In the presence of additional feedback controllers, it is not necessary for the feedforward signal to be excessively accurate; it is sufficient for the controller to
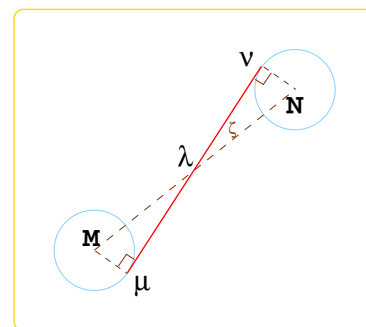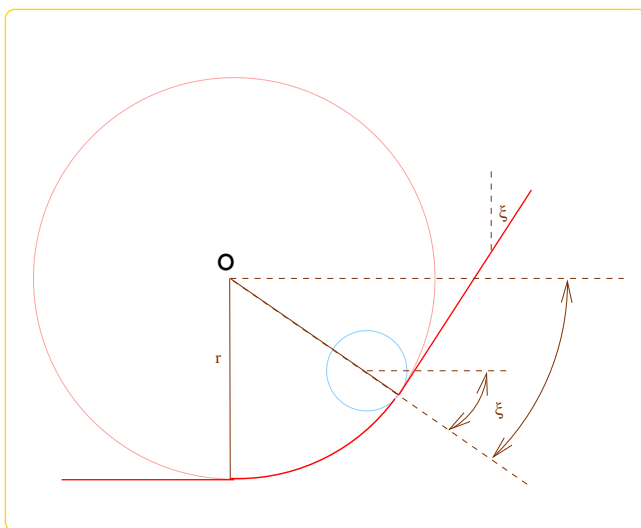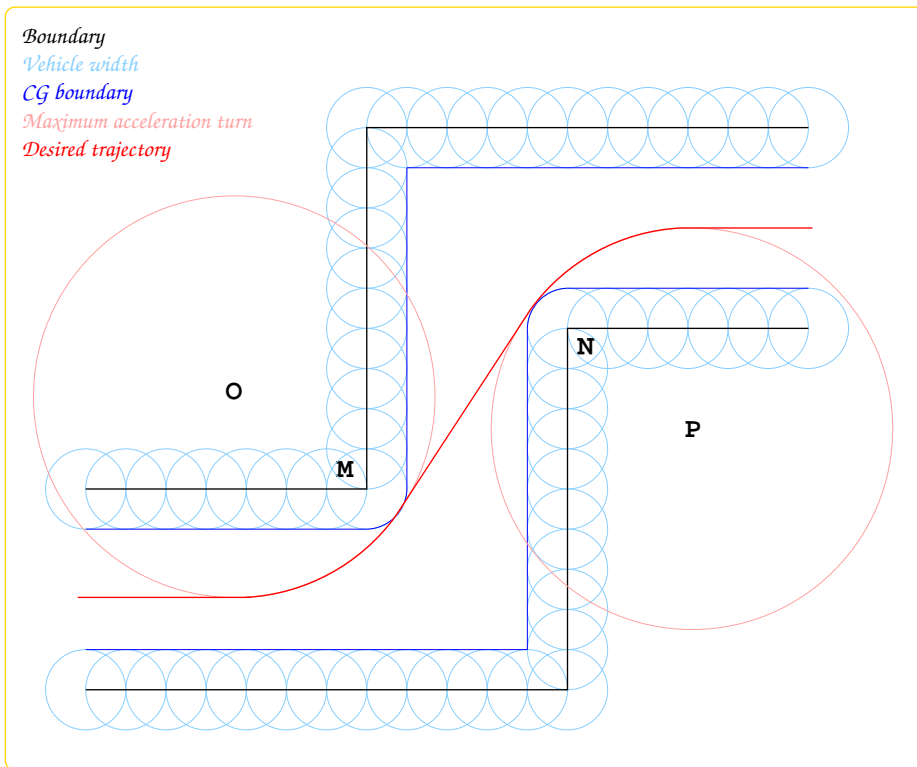
Figure 13: Trajectory generation

A feasible trajectory can be identified by joining circles of radius $r = \frac{\dot{x}^2}{\mu g}$ that keep the vehicle within the spacial limits of the track.

demand a steering angle that will give a reasonable nominal response, allowing the feedback control to cater for unmodelled dynamics. Thus it is desirable to use a simple but robust system model; a one track Ackerman steering model is ideal for the purpose.

The Ackerman steering model is a steady state model which assumes that there is no tyre slip, thus it is dependent only on the geometry of the vehicle. Furthermore, only two parameters are required; the longitudinal moment arms from the centre of gravity (CG) to the front (L_f) and rear (L_r) axles. Even allowing for CG movement due to loading of the vehicle, these parameters will not change greatly from measurements that are known accurately at the time of vehicle production.
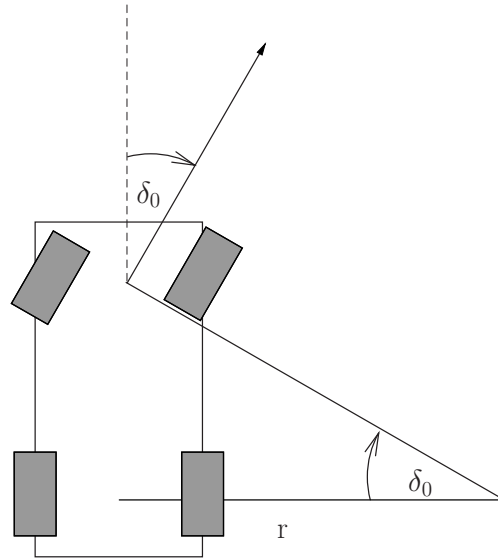
Figure 14: Ackerman steering model

A linear one-track (bicycle) model which assumes no slip and approximates low-speed steady turning of the vehicle where the vehicle wheelbase is much shorter than the radius of curvature.

The steering angle is simply calculated as

$$\delta_0 = \frac{L_f - L_r}{r} \tag{47}$$

where r is the radius of the curvature.

3.5.2   Feedback position control

The feedforward component of the steering control is augmented by a proportional feedback controller

$$u_\Delta = K_\Delta \, e_Y \tag{48}$$

that acts on the error in the vehicle's lateral position, $e_Y = Y_\oplus^* - Y_\oplus$. The gain K_Δ is determined using the procedure described in section 3.7.1

3.6 Brake-by-wire

3.6.1 Feedforward brake pulse

In an emergency it is generally a safe option to apply the brakes and remove energy from the system if the vehicle is equipped with an anti-lock braking system. The purpose of this work is to develop a controller which can be used when braking is not the best option because there is insufficient space to stop. However, even in this case it is beneficial to apply the brakes and reduce the vehicle speed unless to do so would interfere with steering. The nature of the manoeuvre to be executed precludes steering during part of the approach in section 1 because there is no space adjacent to the vehicle and it is too soon to begin turning if the first corner is to be avoided. Consequently, at the start of the manoeuvre, it is sensible to apply as much braking force as possible; the controller does so. As soon as the vehicle begins turning, this braking action is terminated and any subsequent braking occurs only as demanded by the velocity feedback controller.

3.6.2 Feedback velocity control

A proportional feedback controller,

$$u_b = K_b \, e_\psi \tag{49}$$

acts on the error in the vehicle's yaw rate, $e_\psi = \Psi_\oplus^* - \psi$. After multiplication by the controller gain K_b, which is determined using the procedure described in section 3.7.1, the control signal u_b is allocated to the individual brakes on the basis of a pseudo-inverse model $B_f^\dagger$.

3.6.3 Brake force allocation

The major difficulty with using brakes to stabilise the vehicle yaw rate about the desired trajectory is that of allocating control effort to each of the four actuators. The effect of braking each wheel will vary during the manoeuvre depending on the orientation of each wheel to the vehicle body velocity vector. The front wheels, in particular, will vary considerably as large steering inputs are applied

The control effort can be apportioned between the brakes by weighting the demanded forces using a pseudo-inverse model, $B_f^\dagger$. This model may be dynamic, updated according to the changing vehicle states, or static, pre-determined for a single operating condition.

The manoeuvre is aggressive; large steering inputs will be applied while the vehicle is far from equilibrium conditions. Consequently it is not desirable to attempt to linearise a model in the conventional manner using small perturbations about an equilibrium point because the behaviour of the resultant model is unlikely to be representative of the actual vehicle dynamics when the brakes must be applied. A velocity based linearisation is therefore used instead.

The velocity based linearisation is derived from a two-track model of the form

$$\dot{\mathbf{v}} = f(\mathbf{v}, \delta, \mathbf{f_x}) \tag{50}$$

where $\mathbf{v}$ is a vector of the vehicle velocities $(\dot{x}, \dot{y}, \dot{\psi})$, δ is the front wheel steering angle and $\mathbf{f_x}$ is a vector of the wheel brake forces. Differentiating equation 50 with respect to time yields a linear model in which the vehicle accelerations are states and the rates of the steering angle and brake forces are inputs,

$$\ddot{\mathbf{v}} = \frac{\partial g}{\partial \mathbf{v}}\dot{\mathbf{v}} + \frac{\partial g}{\partial \delta}\dot{\delta} + \frac{\partial g}{\partial \mathbf{f_x}}\dot{\mathbf{f}}_{\mathbf{x}} \tag{51}$$

Substituting $\mathbf{w} = \dot{\mathbf{v}}$, equation 51 can be re-written as

$$\dot{\mathbf{w}} = \mathrm{A}(\rho)\dot{\mathbf{v}} + \mathrm{B}_\delta(\rho)\dot{\delta} + \mathrm{B}_\mathrm{f}(\rho)\dot{\mathbf{f}}_{\mathbf{x}} \tag{52}$$

where $\mathrm{A}(\rho) = \frac{\partial g}{\partial \mathbf{v}}$, $\mathrm{B}_\delta(\rho) = \frac{\partial g}{\partial \delta}$, $\mathrm{B}_\mathrm{f}(\rho) = \frac{\partial g}{\partial \mathbf{f_x}}$ and ρ is a scheduling vector comprising necessary states and inputs; in this case $\rho = (\mathbf{v}, \delta)^T$.

The force input matrix B_f is not square and cannot therefore be inverted directly. However, a pseudo-inverse can readily be performed to produce a matrix suitable for use as the control allocation weighting. When performing a pseudo-inversion of a matrix, a tolerance must be provided below which singular values will be neglected. Matrix algebra tools such as Matlab and Octave often have this value set close to the machine limit of precision. A control allocation block produced from a pseudo-inversion using such a low tolerance may generate excessively large outputs. Good results have been obtained using a tolerance which is the recipricol of the approximate maximum brake force that might be applied to a wheel, i.e. tol $= 4/(mg)$ where m is the mass of the car.

3.7 Design procedure

3.7.1 Feedback gain tuning

Linear design methods such as pole-placement and loop-shaping were used to obtain gains for the feedback loops. When tested with a non-linear model it was immediately clear that the performance of the controllers was not at all close to that desired. Moreover, when reasonable controller gains were obtained at a particular operating point using manual tuning, no justification for the resultant values could be found when applied to the linear models. It became clear that the linear model (obtained using velocity-based linearisation) failed to capture some important dynamic effect within the system. Inspection of the nonlinear and linearised models suggests that a likely reason is the multiplication of inputs in the nonlinear system which is not adequately captured when using a selected operating condition to design the gains; the plant changes too dramatically during the manoeuvre for such gains to be appropriate over a useful range to encompass the manoeuvre.

The controller was therefore developed in a manner that would not suffer from limitations inherent in linearised models. A cascade design process was used with iterative refinement, entailing use of non-linear models, to tune two proportional gains.

Initial evaluation was performed using the non-linear model developed in work package 1.2, reported in deliverable D7. Verification of the results, with some minor refinement, was then performed using the detailed proprietary model provided by DaimlerChrysler.

The following steps describe the process used, one which it is believed will be suitable for similar design tasks.

Trajectory generation The first step in the design process is to define a feasible trajectory, i.e. one that will allow the car to perform the specified manoeuvre while respecting spatial and dynamic constraints.

A boundary on the permissible position of the vehicle centre of gravity (CG) can be obtained by defining circles with a radius equal to the width of the car at each point along the specified limits of the manoeuvre area. As long as sufficient space is available for the manoeuvre to be achievable (at any speed), the sides of the vehicle will not exceed the manoeuvre boundary if the CG does not enter the region enveloped by the circles and the vehicle orientation remains tangential to its outer limit.

A desired locus for the CG can then be described within the subset of the manoeuvre area that does not fall within the prohibited region. To ensure the feasibility of the trajectory, it is necessary to ensure that the radius of curvature at any point on it is greater than the minimum radius of curvature that the vehicle is capable of performing. This can be achieved by using arcs of circles or ellipses with a minimum radius $r = \frac{\dot{x}^2}{\mu g}$, possibly joined by straight lines, to construct the manoeuvre, as shown in figure 13.

Feedforward steering controller After a feasible trajectory has been defined, a feedforward steering controller can be constructed, using an inverse linear steady state model, i.e. the one-track Ackerman steering model given in equation (47), to define the front wheel steering angle δ_0 as a function of the vehicle's longitudinal position ($X_\oplus$) with respect to the Earth.

Simulation with a simple nonlinear design model A simple nonlinear two-track design model should be used for the next phases of the design process.

Test the feedforward controller Applying only the steering profile $\delta_0(X_\oplus)$ to the model, a simulation should be run to ensure that the vehicle responds reasonably at a range of speeds. Unmodelled dynamics and external disturbances will mean that the vehicle will probably not meet the specified manoeuvre requirements at this stage. It is unlikely, for example, that the vehicle will end the manoeuvre on the centreline of the new lane, or even with the correct heading angle.

If the manoeuvre is particularly challenging, it is also to be expected that the vehicle will not achieve the desired maximum yaw rate and will thus not move as far laterally as required.

However, it can be verified that the vehicle starts and finishes turns at the correct place, and in the correct direction. It should also be apparent whether the defined trajectory is appropriate or whether changes need to be made, perhaps to smooth any discontinuities or to correct for implementation errors.

Develop the braking proportional feedback loop Leaving the feedforward controller active, a proportional feedback loop (equation (49)) should be inserted to apply the brakes in response to a yaw rate error signal. The pseudo-inverse model $B_f^\dagger$ is computed and inserted between the control signal u_b and the braking subsystem. In this early part of the design phase, it may be beneficial to have this matrix updated continually during simulations of the manoeuvre to ensure that it is always appropriate for the operating condition of the vehicle.

The proportional gain K_b can now be manually tuned by evaluating the overall performance of the manoeuvre by the vehicle during simulations. The purpose of this control loop is to enhance the vehicle's ability to track the desired yaw rate, so particular attention should be given to performance during curved parts of the trajectory. There may also be some improvement in the final orientation of the vehicle, although it is unlikely that the steady state error will be entirely eliminated.

Develop the steering proportional feedback loop With the brake control loop in place, and the feedforward steering loop still active, a proportional feedback control loop (equation (48)) can be developed to augment the feedforward steering angle input, δ_0.

The purpose of this control loop is to eliminate error in the lateral position of the vehicle, and in particular to ensure that the vehicle correctly finds the centreline of the new lane at the end of the manouevre. Using simulations to tune the gain K_Δ, it is desirable to pay attention to the effect throughout the manoeuvre on the control inputs demanded by the brake controller, in response to any changes in the steering gain. A well designed steering loop should slightly reduce the effort demanded from the brakes.

Iteratively tune both feedback gains With the entire controller in place, and all loops active, it is worthwhile to fine tune the two proportional gains, K_b and K_Δ, in an iterative manner to reduce any fighting between the controllers. The objective should be to reduce the overall control effort demanded by each of the feedback loops.

Tune the controller with a more complex evaluation model The following steps are performed using the more complex evaluation model. It would also be worthwhile to repeat these steps when applying the controller to a real vehicle.

Test the feedforward steering profile Repeating the first step that was performed with the simpler model, a sanity check should be performed to ensure that the vehicle behaves similarly when subjected to the imposed steering profile δ_0 with all other loops inactive. This should quickly identify any major inconsistencies between the models.

Fine tune the complete controller Activating all of the control loops, the vehicle should respond well to the entire controller if there are no major inconsistencies between the two models. If the response is similar to that

achieved with the simpler design model then a straightforward process of fine tuning the two controller gains can be used to further improve the vehicle performance.

If the controller does not work well, it may be necessary to repeat all of the steps that had been performed previously with the design mode, but using the evaluation model instead. However, this should not be necessary unless the design model does not adequately represent the system.

Adapt the controller for real time operation With a fully functioning controller that meets the required specifications, effort can be applied to improve its implementation to make it more suitable for embedding within a real time system.

An obvious improvement is to eliminate the continual re-calculation of the force allocation matrix $B_f^\dagger$. This can be achieved using a scheduling approach and pre-calculating the matrix for a limited number of operating conditions. For the manoeuvre specified in this work, and with the rest of the controller in place, a single operating point suffices. However, it should be noted that this single operating point would not have been sufficient earlier in the design process before the control loops had been implemented and fine-tuned.

If any of the reference inputs or the feedforward steering profile have been implemented in a manner that required calculation throughout the manoeuvre, it is appropriate at this stage to re-implement them as predetermined look-up tables that will not impose an excessive computational load on the processor during the manoeuvre.
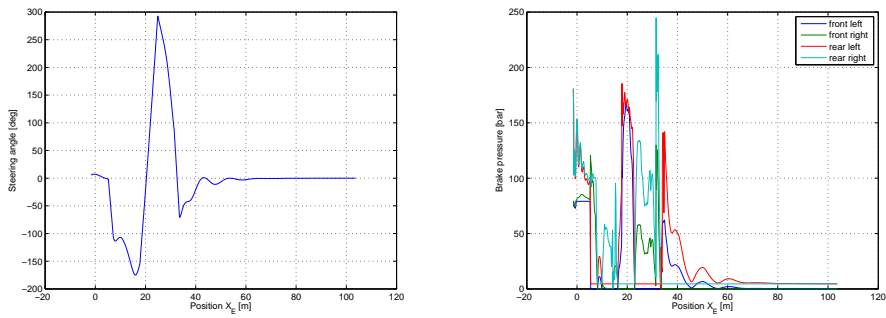
3.8   Simulation results

Evaluation of the controller was performed using a proprietary non-linear model embedded within a Simulink harness. The steering angle and brake pressures output by the controller are shown in figure 15, along with the resultant vehicle trajectory, forward speed and yaw angle.

As explained in section 3.1, for a lateral emergency collision avoidance manoeuvre it should generally be safer to remain in the new lane than to attempt to rejoin the existing one. However, for demonstration of the successful performance of the controller, simulations have also been run using the full manoeuvres specified in ISO 3888. The simulation results are shown in figures 15, 16 and 17.

3.8.1   Discussion

For each of the three manoeuvres demonstrated in figures 15, 16 and 17, it can be seen that the vehicle successfully follows the reference trajectory.

It can be seen that the brakes on each side of the vehicle generally tend to operate synchronously during each of the manoeuvres. This is to be expected because the brakes are being used to control the yaw rate. The magnitude of the brake pressure applied front and rear on either side varies because of several factors:

(a) Steering angle

(b) Brake pressure
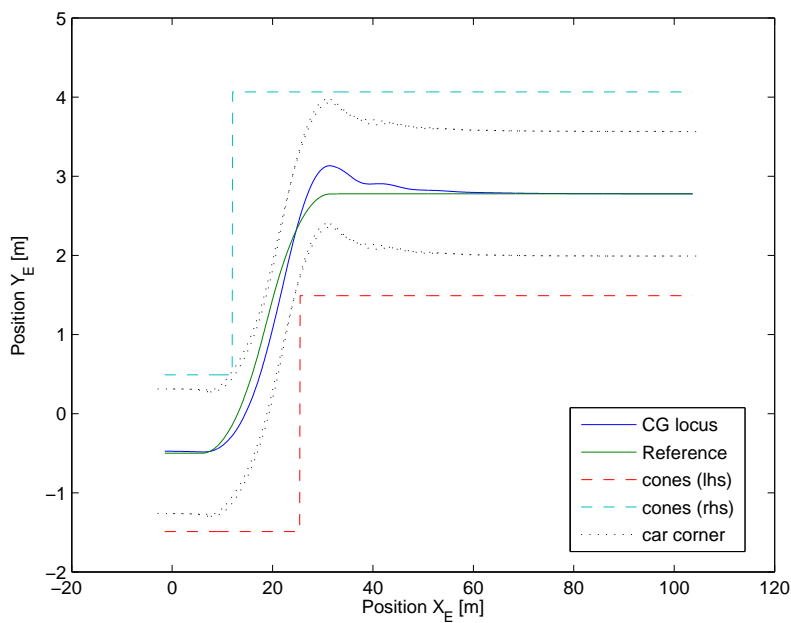
(c) Trajectory

(d) Forward speed

(e) Yaw angle

Figure 15: Simulation results for a single lane change manoeuvre based on the obstacle avoidance manoeuvre defined in ISO 3888-2 [14], starting at 80 [km/hr].
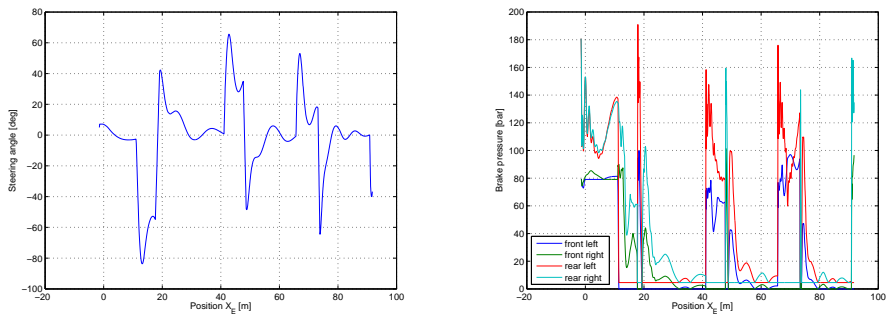
(a) Steering angle
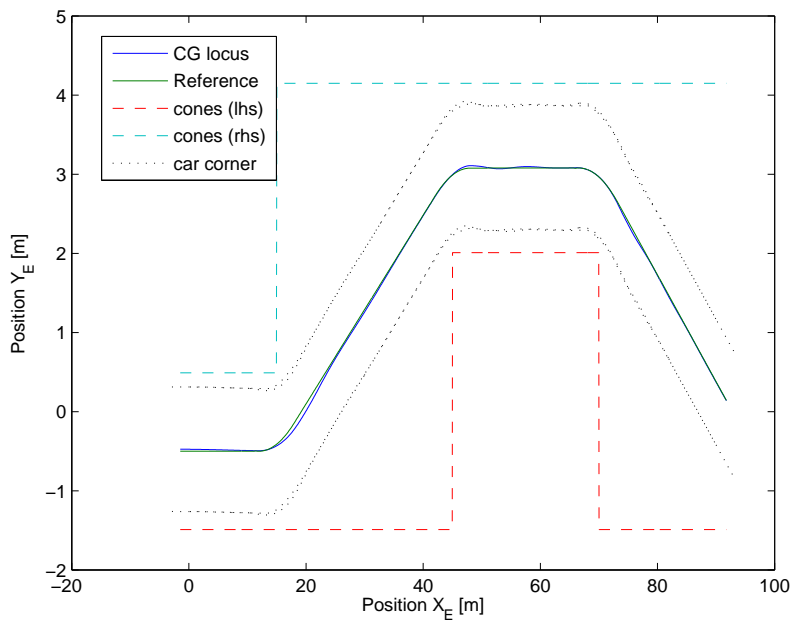
(b) Brake pressure

(c) Trajectory

(d) Forward speed

(e) Yaw angle

Figure 16: Simulation results for the double lane change manoeuvre defined in ISO 3888-1 [13], starting at 80 [km/hr].
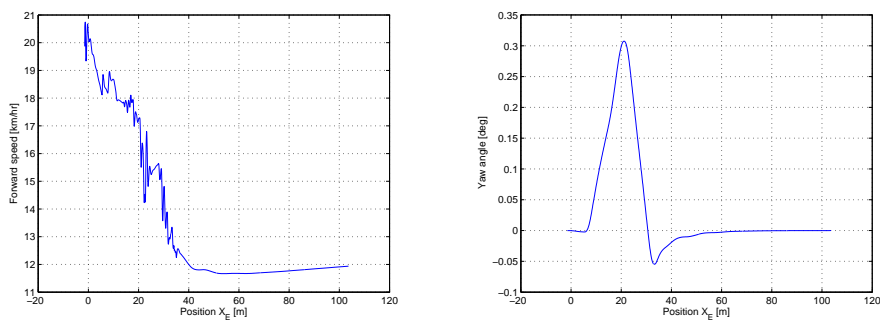
(a) Steering angle

(b) Brake pressure

(c) Trajectory

(d) Forward speed
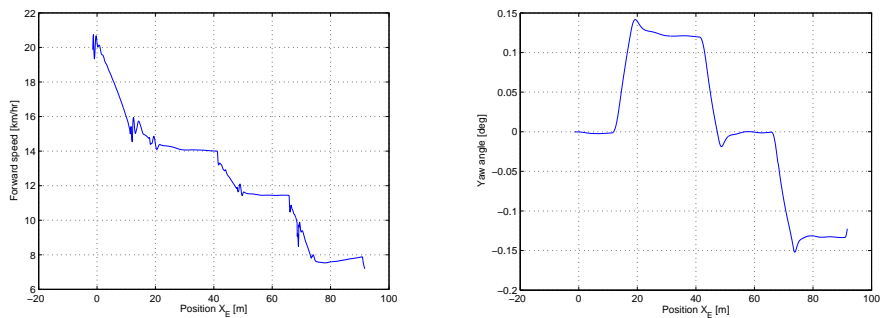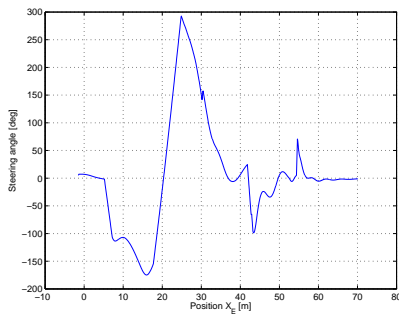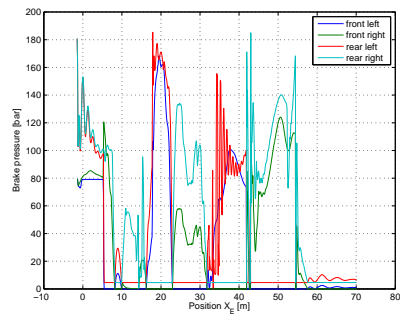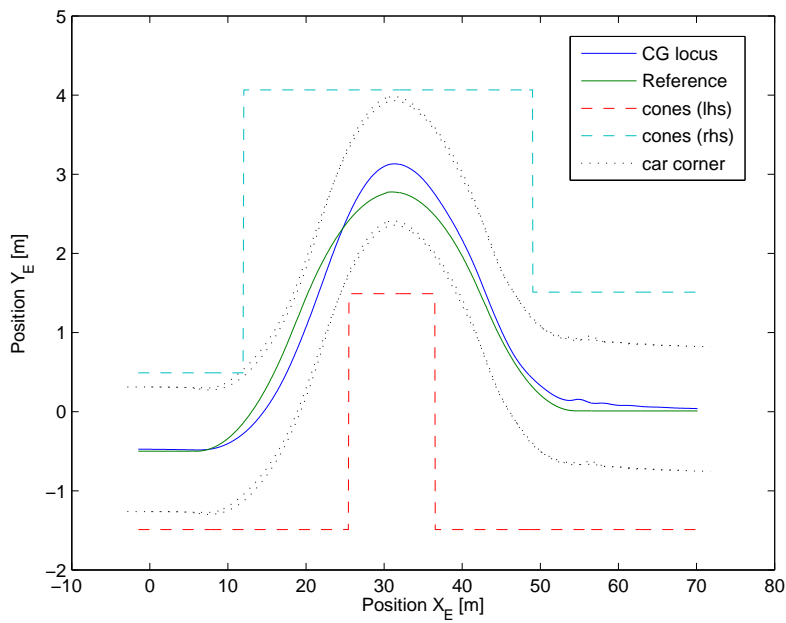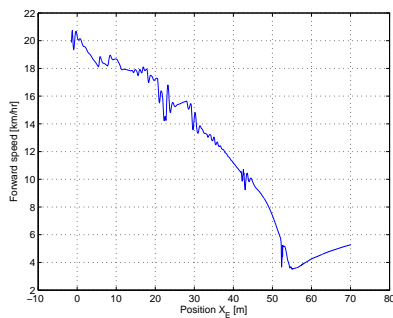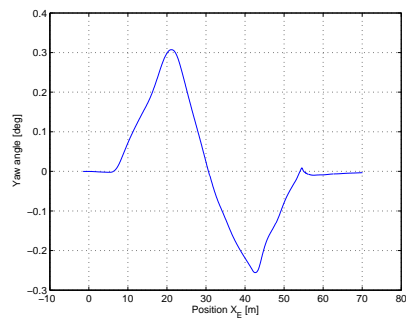

(e) Yaw angle

Figure 17: Simulation results for the obstacle avoidance manoeuvre defined in ISO 3888-2 [14], starting at 80 [km/hr].

- The geometry of the vehicle means that longitudinal forces applied to front and rear wheels provide different contributions to the yaw moment about the vehicle's centre of gravity.

- The effect of braking a front wheel depends on its steering angle. In particular, the direction of the wheel affects whether longitudinal brake forces will help or hinder the turn.

- The mechanical construction of the braking system, with larger brake discs on the front of the vehicle, mean that a given brake force requires lower pressures to be applied to the front wheel than the rear. During heavy braking, load transfer to the front wheels would also add to this effect but this is not included in the inverse model used to allocate the brake forces.

The speed decreases significantly throughout each manoeuvre. Following some initial deceleration due to an explicit feedforward application of the brakes, most of the loss of speed occurs while the brakes are being used to stabilise the vehicle yaw rate through the turns.

The speed increases slightly when no brake pressure is applied due to a small engine torque which is not entirely cancelled by the controller. This could be eliminated, if desired, by feeding an engine torque measurement signal to the brake controller. Alternatively, additional engine torque could be used to control the vehicle speed, as might be desired in a non-emergency lateral controller for joining a stream of traffic in a cruise-control mode.

3.9   Conclusion

Work undertaken within work package 3 has supported the development of a controller for application in work package 1.2. The controller successfully performs the specified single lane-change manoeuvre as well as the double lane change manouevres specified in ISO 3888. Demonstration of the successful performance of the controller supported by this work will be demonstrated by simulation as part of deliverable D13.

4   Dynamic Control Allocation Algorithm for Yaw Stabilization of an Automotive Vehicle using Brakes (WP 1)

In this section we present a yaw stabilization scheme for an automotive vehicle, that has been implemented in a realistic nonlinear multi body vehicle simulation environment. The stabilization strategy is based on two modules independent in design, a high level module that deals with the motion control objective and a low level module that deals with the actuator control allocation. The high level module consists of yaw-rate reference generator and high level controller that provides the low level control allocation module with a desired torque about the yaw axis. The task of the low level module is to command the individual brakes, the longitudinal

clamping force, such that the actual torque about the yaw axis tends to the desired torque. These commands are generated by a dynamic control allocation algorithm that also takes actuator constraints and uncertainty in the tyre-road friction model into consideration. Simulation cases where the tyre-road friction parameter was considered both known and unknown, show that the control scheme stabilizes the vehicle in extreme manoeuvres where the nonlinear vehicle yaw dynamics otherwise becomes unstable in the sense of over- or under-steering.

4.1   Introduction

Some of the major advances in automotive technology in the past decade have been in the area of safety, and most modern passenger vehicles are now equipped with an active safety system. Important components in these systems are Anti-lock Braking Systems (ABS), Traction Control Systems/Antispin (TCS) and recently Electronic Stability Programs (ESP). ABS and TCS are systems designed to maximize the contact-force between the tyres and the road during braking and acceleration, while ESP is introduced in order to control the yaw motion directly and prevent skidding. The yaw dynamic may be controlled by active steering [15], [16], [17], [18] and [19] or active braking [20], [21] and it is in [22] shown that the knowledge of the friction coefficient offers significant improvement of the vehicle response during yaw rate control.

In this work we present a yaw stabilization schemes for an automotive vehicle using brakes, based on the dynamic optimizing control allocation approach presented in [23] and [24]. This strategy offers the benefits of a modular approach of combining convergence and stability properties for yaw rate tracking, optimality of the allocation problem and adaptation of the maximal tyre-road friction parameter (section II). In [25] and [26] the control allocation problem is solved statically by a real-time optimizing program. By solving the control allocation problem dynamically (not necessarily finding the optimal solution at each sampling instant) a real-time implementation can be realized without the use of any numeric optimization software. In general, this is an advantage since implementations on vehicles with low-cost hardware may be considered.In [27] an explicit piecewise linear approximate solution is created by using multiparametric programming and solving the optimization problem off-line. As an alternative to this approach the algorithm presented here is founded by a stability proof using Lyapunov functions, a benefit of the approach is low computational complexity due to the asymptotic optimality approach, without any loss of stability properties.

By including an adaptive law for estimating the maximal tyre-road friction parameter, the yaw stabilizing scheme takes changing road conditions into account, and ultimately the control allocation algorithm will perform better.

The theory and results presented here are related to Work-package 1 of the project, concerning active safety systems such as ESP, collision avoidance and rollover protection.

4.2 Background on The Control Allocation Scheme

We have based our yaw stabilizing scheme for the automotive vehicle on designing the control algorithm separately from the allocation algorithm, and we rely on the results presented in [24] and [23] in order to show stability and convergence for our modular design approach. Consider the general nonlinear system (see [24] for technical assumptions) given by

$$\dot{x} = f_1(t,x) + f_2(t,x)\tau \tag{53}$$
$$\tau = \Phi(t,x,u)\theta , \tag{54}$$

where $t > 0$ is the time, $x \in \mathbb{R}^n$ is the state vector, $u \in \mathbb{R}^r$ the control input vector, $\tau \in \mathbb{R}^d$ is the virtual control and $\theta \in \mathbb{R}^m$ is a constant vector of unknown parameters, the system is over-actuated and $m \leq d \leq r$. Then, our construction is based on the following three steps:

1. **The high level control algorithm.** The virtual control τ is treated as an available input to system (53), and a virtual control law $\tau_c := k(t,x)$ is designed such that the origin of system (53) is UGAS.

2. **The control allocation algorithm.** Based on the minimization problem

$$\min_u J(t,x,u) \quad s.t. \quad k(t,x) - \Phi(t,x,u)\theta = 0 , \tag{55}$$

where $J(t,x,u)$ is a cost function that incorporates objectives such as minimum power consumption and actuator constraints (implemented as barrier functions), the Lagrangian function

$$L(t,x,u,\lambda) = J(t,x,u) + (k(t,x) - \Phi(t,x,u)\theta)^{\mathrm{T}}\lambda \tag{56}$$

is introduced, and update laws for the control input u and the Lagrangian parameter λ are then defined such that u and λ converges to a set defined by the first order optimality condition on L.

3. **The adaptive law.** In order to cope with an unknown parameter vector θ in the effector model, an adaptive law is defined. The parameter estimate is used in the control allocation algorithm and a certainty equivalent adaptive optimal update law can be defined.

4.3 Vehicle model

Our yaw stabilization scheme design is based on an horizontal plane two-track model that can be found in [28]. The structure of this model is given by

$$\dot{x} = f_1(x) + f_2(x)\tau \tag{57}$$
$$\tau = \Phi(\alpha, u, \delta, \mu_H) , \tag{58}$$

where $x := (\nu, \beta, r)^{\mathrm{T}}$, $\tau := (f_x, f_y, M)^{\mathrm{T}}$ and $u := (\lambda_{x1}, \lambda_{x2}, \lambda_{x3}, \lambda_{x4})^{\mathrm{T}}$. Specifically the dynamic part of the model takes the form
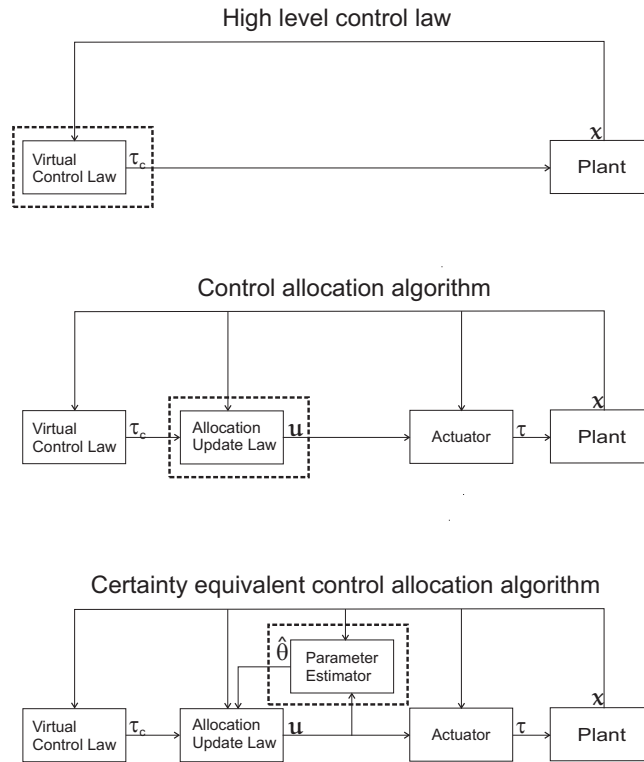
Figure 18: The modular steps of constructing the control scheme

Nomenclature	
ν	Absolute velocity at the CG of the vehicle
β	Vehicle side slip angle
ψ	Yaw
r	Yaw rate ($\dot{\psi}$)
F_{xi}	Friction force on wheel in longitudinal wheel direction
F_{yi}	Friction force on wheel in lateral wheel direction
F_{zi}	Vertical force on ground from each wheel
δ_i	Steering angle
M	Torque around the yaw axis
M_d	Desired torque around the yaw axis
m	Vehicle mass
J_z	Vehicle moment of inertia about CG
μ_H	Maximum tyre-road friction coefficient
μ_y	Lateral tyre-road friction coefficient
μ_x	Longitudinal tyre-road friction coefficient
α_i	Wheel side slip angle
λ_{xi}	Wheel slip in longitudinal wheel direction
ω_i	Angular velocity of wheel i
R	Radius of the wheels

Table 5:
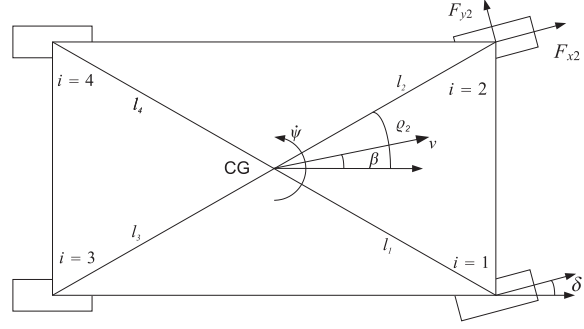
Figure 19: Vehicle geometry [27]

$$f_1(x) := \quad (0, -r, 0)^{\mathrm{T}}$$

$$f_2(x) := \quad \begin{pmatrix} \frac{1}{m}\cos(\beta) & \frac{1}{m}\sin(\beta) & 0 \\ -\frac{1}{m\nu}\sin(\beta) & \frac{1}{m\nu}\cos(\beta) & 0 \\ 0 & 0 & \frac{1}{J_z} \end{pmatrix}$$

while the static actuator model takes the following form

$$\Phi(\alpha, u, \delta, \mu_H) := \begin{pmatrix} \sum_{i=1}^{4} D(\delta_i) \begin{pmatrix} F_{xi} \\ F_{yi} \end{pmatrix} \\ \sum_{i=1}^{4} g^T(l_i, \rho_i) D(\delta_i) \begin{pmatrix} F_{xi} \\ F_{yi} \end{pmatrix} \end{pmatrix},$$

where $\alpha := (\alpha_1, .., \alpha_4)$, $\delta := (\delta_1, .., \delta_4)$ and

$$\begin{pmatrix} F_{xi} \\ F_{yi} \end{pmatrix} (\alpha_i, \lambda_{xi}, \delta_i, \mu_H) \quad : \quad = \begin{pmatrix} -F_{zi}\mu_x(\lambda_{xi}, \alpha_i, \mu_H) \\ F_{zi}\mu_y(\lambda_{xi}, \alpha_i, \mu_H) \end{pmatrix}$$

$$g^T(l_i, \rho_i) \quad : \quad = \begin{pmatrix} -\sin(\rho_i) \\ \cos(\rho_i) \end{pmatrix} h_i$$

$$D(\delta_i) \quad : \quad = \begin{pmatrix} \cos(\delta_i) & -\sin(\delta_i) \\ \sin(\delta_i) & \cos(\delta_i) \end{pmatrix}$$

$$\lambda_{xi} \quad : \quad = \frac{\nu - \omega_i R}{\nu} ,$$

and l, h, R and ρ are vectors with geometrical parameters of the vehicle. See Figure 19 and Table 5 for parameter explanation.

4.4 Yaw Stabilization

The control objective is to prevent the vehicle from over- or under-steering, i.e. the yaw rate, r, of the vehicle should be close to some desired yaw rate, r_{ref}, defined by the commanded steering angle. In order to generate this reference the steady-state of the side-slip dynamics is considered. Thus from the model

$$\dot{\beta} = -r + \frac{-\sin\beta f_x + \cos\beta f_y}{\nu} ,$$

where $(f_x, f_y)^{\mathrm{T}} := \sum_{i=1}^{4} D(\delta_i) \, (F_{xi}, F_{yi})^{\mathrm{T}}$, the desired reference,

$$r_{ref} := \frac{f_y(\alpha, 0, \delta, \mu_{dH})}{v}, \tag{59}$$

is generated by letting $\dot{\beta} = \beta = 0$ and $u = 0$, where μ_{dH} is a desired maximal tyre road friction parameter.

For safe driving [28], the side-slip should be bounded by

$$|\beta| \leq 10° - 7° \frac{\nu^2}{(40[m/s])^2} \ . \tag{60}$$

Although this bound is not explicitly enforced in this scheme, simulations show that the side-slip is bounded as long as the yaw reference is followed.

The high-level control design (the desired torque trajectory construction) is based on the reduced model:

$$\dot{r} = \frac{M}{J_z} \ . \tag{61}$$

Let $\eta := r - r_{ref}$ denote the error-state such that the tracking problem can be described by

$$\begin{aligned} \dot{\eta} &= \frac{M}{J_z} - \dot{r}_{ref}(t) \\ &= -\frac{K}{J_z}\eta + \frac{M - M_d}{J_z} \ , \end{aligned} \tag{62}$$

where $M_d := -K\eta + J_z \dot{r}_{ref}(t)$ is the suggested virtual control law. With $M = M_d$ the tracking error dynamics is, linearly described, by:

$$\dot{\eta} = -\frac{K}{J_z}\eta \ . \tag{63}$$

Thus the origin of (63) is uniformly globally exponential stable for $K > 0$.

4.5 Dynamic control allocation algorithm

The basis of the control allocation algorithm lies in finding an update law for the longitudinal wheel-slip (λ_{xi}) that asymptotically solves the optimization problem

$$\min_u J(u) \quad s.t. \ M_d(t, \eta) - \bar{M}(t, u, \mu_H) = 0 \ , \tag{64}$$

where $M_d(t, \eta)$ is the virtual control (desired torque) and $\bar{M}(t, u, \mu_H) := M(\alpha(t), u, \delta(t), \mu_H)$ is the torque achieved by manipulating u. The instantaneous cost function is divided into two parts, $J(u) := J_1(u) + J_2(u)$, where the function $J_1(u)$ represents the actuator penalty and the $J_2(u)$ is a barrier function representation of the actuator

constraints.

$$J_1(u) \quad : \quad = u^{\mathrm{T}} \Gamma_u u \tag{65}$$

$$J_2(u) \quad : \quad = -w_u \sum_{i=1}^{4} \ln(\lambda_{xi} - \lambda_{x\,\min})$$

$$-w_u \sum_{i=1}^{4} \ln(-\lambda_{xi} + \lambda_{x\,\max}) \;, \tag{66}$$

where $\lambda_{x\,\max}$ and $\lambda_{x\,\min}$ are wheel-slip constraints and Γ_u and w_u are weighting parameters. The Lagrangian function for problem (64) is

$$L(t, \eta, u, \lambda) = J(u) + (M_d(t, \eta) - \bar{M}(t, u, \mu_H))^{\mathrm{T}} \lambda \tag{67}$$

where λ is the lagrangian parameter. The first order optimality condition is defined by the sets

$$\mathcal{O}_0(t, \eta) \quad : \quad = \left\{ u \in U, \lambda \in \mathbb{R} \,\middle|\, \frac{\partial L}{\partial u} = 0, \frac{\partial L}{\partial \lambda} = 0 \right\} \tag{68}$$

$$U \quad : \quad = [\lambda_{x\,\min}, \lambda_{x\,\max}]^4 \;. \tag{69}$$

Consider applying a Newton like update-law of the same from as in [23]

$$\left(\dot{u}, \dot{\lambda} \right)^{\mathrm{T}} = -\gamma \left(\mathbb{H}^{\mathrm{T}} \mathbb{H} + \varepsilon I_{r+p} \right)^{-1} (\alpha_u, \beta_u)^{\mathrm{T}} + (\zeta, \phi)^{\mathrm{T}} \tag{70}$$

where ζ and ϕ solves the equation

$$\alpha_u^{\mathrm{T}} \zeta + \beta_u^{\mathrm{T}} \phi + \delta_u = 0 \tag{71}$$

Moreover $\mathbb{H} := \begin{pmatrix} \frac{\partial^2 L}{\partial u^2} & -(\frac{\partial M}{\partial u})^{\mathrm{T}} \\ -(\frac{\partial M}{\partial u}) & 0 \end{pmatrix}$, $\varepsilon > 0$ and $\gamma = \gamma^T \in \mathbb{R}^{5\times5}$ is a positive definite matrix. And

$$\alpha_u \quad : \quad = \frac{\partial^2 L}{\partial u^2} \frac{\partial L}{\partial u} - b^2 \frac{\partial M^{\mathrm{T}}}{\partial u} \frac{\partial L}{\partial \lambda} \tag{72}$$

$$\beta_u \quad : \quad = -\frac{\partial M}{\partial u} \frac{\partial L}{\partial u} \tag{73}$$

$$\delta_u \quad : \quad = (\frac{\partial l^{\mathrm{T}}}{\partial u} \frac{\partial^2 L}{\partial \eta \partial u} + b^2 \frac{\partial L^{\mathrm{T}}}{\partial \lambda} \frac{\partial^2 L}{\partial \eta \partial \lambda}) M$$

$$+ \frac{\partial L^{\mathrm{T}}}{\partial u} \frac{\partial^2 L}{\partial t \partial u} + \frac{\partial L}{\partial \lambda} \frac{\partial^2 L}{\partial t \partial \lambda} \;, \tag{74}$$

where $b > 0$ is a design parameter shaping (75). This parameter is chosen such that the deviation of $\left| \frac{\partial L}{\partial \lambda} \right| = \left| M_d(t, \eta) - \bar{M}(t, u, \mu_H) \right|$ from zero, is penalized more then the deviation of $\left| \frac{\partial L}{\partial u} \right|$ from zero, in the search direction described by (70). The set $\mathcal{O}_0(t, 0)$ can be proved uniformly exponentially stable by showing that the Lyapunov function candidate

$$V_1(t, \eta, u, \lambda) := \sigma \frac{\eta^2}{2} + \frac{1}{2} \left(\frac{\partial L^{\mathrm{T}}}{\partial u} \frac{\partial L}{\partial u} + b^2 \frac{\partial L^{\mathrm{T}}}{\partial \lambda} \frac{\partial L}{\partial \lambda} \right) \;, \tag{75}$$

where $\sigma > 0$, in fact is a Lyapunov function for set $\mathcal{O}_0(t, 0)$ with respect to system (62) and (70).

---

4 Control Allocation for Yaw Stabilization (WP 1)

Remark 1 *Note that the implementation of the control allocation update law (70) requires that the states are known. In addition, this is only a local result since V_1 is not defined for $u \notin U$. For details see [24] and assume that all parameters are known.*

4.6   Adaptive law and certainty equivalent allocation algorithm

The actuator model is dependent on the maximal friction coefficient, μ_H, between the tyres and the road. This parameter is dependent on the road conditions that is not easily monitored, thus it might be useful to construct an estimate, $\hat{\mu}_H$, of this parameter. We assume that the maximal tyre-road friction parameter is equal for each wheel, but since μ_H is not affine in the vehicle actuator model (58), the adaptive law from [24] can not be used directly. In order to get a model representation that is affine in μ_H the following Taylor series expansion is considered.

$$
\begin{aligned}
\bar{M}(t,u,\mu_H) &= \bar{M}(t,u,\hat{\mu}_H) + \left.\frac{\partial \bar{M}(t,u,\xi)}{\partial \xi}\right|_{\xi=\hat{\mu}_H} \tilde{\mu}_H \\
&+ \left.\frac{\partial^2 \bar{M}(t,u,\xi)}{\partial \xi^2}\right|_{\xi=\hat{\mu}_H+\varsigma\tilde{\mu}_H} \frac{(\tilde{\mu}_H)^2}{2}
\end{aligned}
\tag{76}
$$

for some $0 \le \varsigma \le 1$. Further the optimization problem takes the form

$$
\min_u J(u) \quad s.t. \quad M_d(t,\eta) - \bar{M}(t,u,\hat{\mu}_H) = 0 \ ,
\tag{77}
$$

such that the belonging Lagrangian function is given by

$$
\hat{L}(t,\eta,u,\lambda,\hat{\mu}_H) = J(u) + (M_d(t,\eta) - \bar{M}(t,u,\hat{\mu}_H))^{\mathrm{T}} \lambda \ .
\tag{78}
$$

Based on the estimate

$$
\dot{\hat{r}} = A(r - \hat{r}) - \bar{M}(t,u,\hat{\mu}_H)
\tag{79}
$$

where $A > 0$, we get the adaptive law

$$
\dot{\hat{\mu}}_H = \Gamma_{\mu_H} \left.\frac{\partial \bar{M}(t,u,\xi)}{\partial \xi}\right|_{\xi=\hat{\mu}_H} e
\tag{80}
$$

$$
e := \delta_\theta + \epsilon^T Q_\epsilon \ ,
\tag{81}
$$

where $\epsilon := r - \hat{r}$, $\delta_\theta := \frac{\partial \hat{L}^T}{\partial u}\frac{\partial^2 \hat{L}}{\partial \eta \partial u} + \frac{\partial \hat{L}^T}{\partial \lambda}\frac{\partial^2 \hat{L}}{\partial \eta \partial \lambda} + \sigma\eta$ is a feed-forward term that will help insuring stability of the adaptive law, and $\Gamma_{\mu_{H1}} > 0$. This adaptive law has the same structure as presented in [24], and the uniformly asymptotic stability (UAS) properties of set $\mathcal{A} := \{\epsilon \in \mathbb{R}, \tilde{\mu}_H \in (-1..1) \,|\, \epsilon = 0, \tilde{\mu}_H = 0\} \times \mathcal{O}_0(t,0)$ follows by assuming that $\left.\frac{\partial^2 \bar{M}(t,u,\xi)}{\partial \xi^2}\right|_{\xi=\hat{\mu}_H+\varsigma\tilde{\mu}_H}$ from (76) is bounded.

The adaptive control allocation algorithm is obtained by implementing the certainty equivalent of (70), where μ_H is replaced with $\hat{\mu}_H$ and

$$
\begin{aligned}
\delta_u = \delta_{u\mu_H} := {} & \frac{\partial \hat{L}^T}{\partial \lambda} \frac{\partial^2 \hat{L}}{\partial t \partial \lambda} + \frac{\partial \hat{L}^T}{\partial u} \frac{\partial^2 \hat{L}}{\partial t \partial u} \\
& + \left(\frac{\partial \hat{L}^T}{\partial u} \frac{\partial^2 \hat{L}}{\partial \hat{\mu}_H \partial u} + \frac{\partial \hat{L}^T}{\partial \lambda} \frac{\partial^2 \hat{L}}{\partial \hat{\mu}_H \partial \lambda} \right) \dot{\hat{\mu}}_H \\
& + \left(\frac{\partial \hat{L}^T}{\partial u} \frac{\partial^2 \hat{L}}{\partial \eta \partial u} + \frac{\partial \hat{L}^T}{\partial \lambda} \frac{\partial^2 \hat{L}}{\partial \eta \partial \lambda} \right) \frac{\bar{M}(t, u, \hat{\mu}_H)}{J_z} .
\end{aligned}
\tag{82}
$$

4.7 Implementation and simulation results

In order to validate the yaw stabilization scheme, a test-bench based on Daimler-Chrysler's proprietary simulation environment CASCaDE (Computer Aided Simulation of Car, Driver and Environment) for MATLAB, is considered. The simulation scenarios are based on the non controlled "unstable" behavior of a vehicle undergoing the steering manoeuvre shown in Figure 20, where the tyre-road friction is set to $\mu_H = 0.5$. The vehicle output/measurements are sampled with a $100 Hz$ sam-
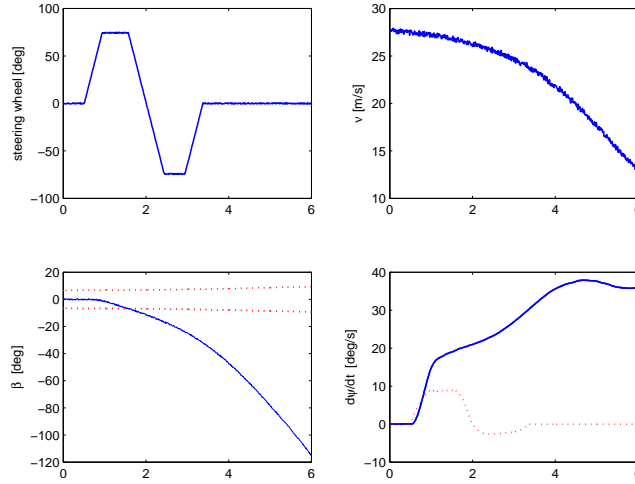
Figure 20: Simulation without the yaw stabilizing scheme. The dotted lines are given by $|\beta|_{max}$ (60), and r_{ref} (59).

pling rate, and the control module (yaw stabilization algorithm) has an input and output sampling rate of $50 Hz$ and the actuators are implemented with a delay of 0.01 seconds. The algorithm parameters used in the simulations are given by Table 6. In order to prevent the allocation update law (70) and its certainty equivalent law from generating infeasible actuator commands, due to the discretization of the system, γ is chosen to be a diagonal matrix where each element represents a positive step length that is made as small as necessary to achieve feasibility.

The CASCaDE model control inputs are defined through the steering angle and an ABS control module where desired brake force (F_{xi_des}) for each wheel in the

Algorithm parameters	
ε	10^{-8}
σ	1
b	8
Γ_u	$10^3 I_{4\times4}$
K	$20 J_z$
$\lambda_{x\,\min}$	-10^{-5}
$\lambda_{x\,\max}$	$0.12 + 10^{-5}$
w_u	1
$\Gamma_{\mu_{H1}}$	$2 \cdot 10^{-7}$
$\Gamma_{\mu_{H2}}$	$5 \cdot 10^{-7}$
A	200
Q_ϵ	$A J_z$

Table 6:

longitudinal direction can be specified. These forces are generated by inserting the desired solution of the control allocation problem (updated wheel-slip) in the friction model. The simulation results are presented in figures 21-24 and the control objective (yaw-rate reference tracking and steerability conservation) is satisfied in both the nonadaptive and the adaptive scheme. Figure 5 and 7 should be understood as follows: The real torque around the yaw axis $M_{measured}$ is tracked by $\bar{M}(t, u, \hat{\mu}_H)$ due to the adaptive law, but since $\bar{M}(t, u, \hat{\mu}_H)$ also tracks the virtual control M_d due to the dynamic control allocation algorithm, $M_{measured}$ should track M_d.

The adaptive algorithm seem to perform better then the nonadaptive in the sense of yaw rate reference following, also the measured wheel-slip seem to follow the commanded wheel-slip better.

4.8 Concluding remarks

4.8.1 Conclusion

Based on a dynamic adaptive control allocation algorithm a yaw stabilizing scheme for an automotive vehicle was proposed. The scheme performed well when implemented on a realistic nonlinear simulation environment. Both due to linearization and structural model errors (the simulation environment model is not known) the estimate representing the maximal tyre-road friction parameter does not necessarily converge to the real value, but the over all performance of the adaptive scheme tends to be more efficient in the sense of satisfying the control objective.

4.8.2 Further work

- Include steering angle and active suspension in the design.

- Design adaption laws for the maximal tyre-road friction parameter on each wheel.

Also in order to validate the results, tests on a real vehicle are considered.

(a) States. The dotted lines are given by $|\beta|_{max}$ (60), and r_{ref} (59)

(b) Real wheel-slip (dotted line) and desired wheel-slip (solid line) commanded by the allocation algorithm

Figure 21: Simulation of the nonadaptive algorithm with the maximal tyre-road friction parameter assumed to be constant $\hat{\mu}_H = 0.8$, while the real value is $\mu_H = 0.5$
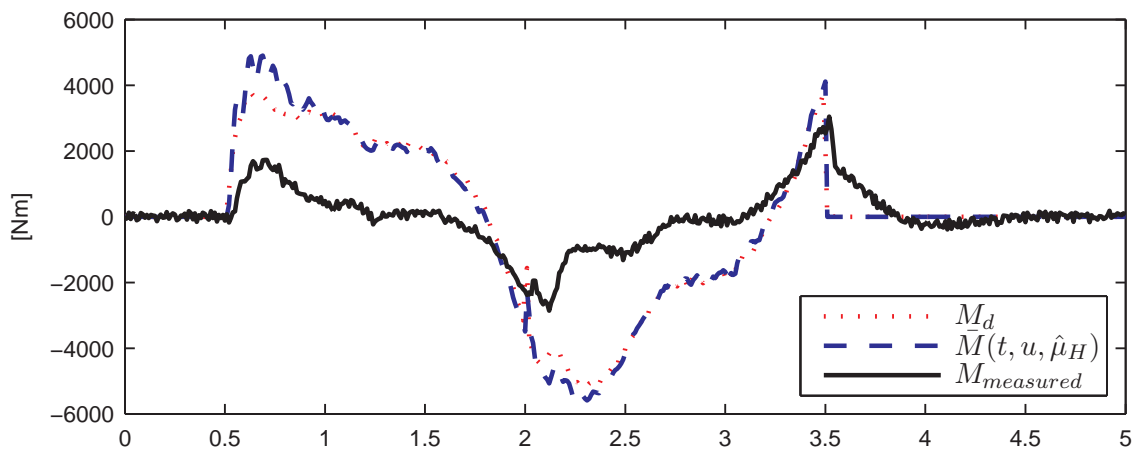
Figure 22: Torque simulation of the nonadaptive algorithm with the maximal tyre-road friction parameter assumed to be constant $\hat{\mu}_H = 0.8$, while the real value is $\mu_H = 0.5$

(a) States. The dotted lines are given by $|\beta|_{max}$ (60), and r_{ref} (59).

(b) Real wheel-slip (dotted line) and desired wheel-slip (solid line) commanded by the allocation algorithm
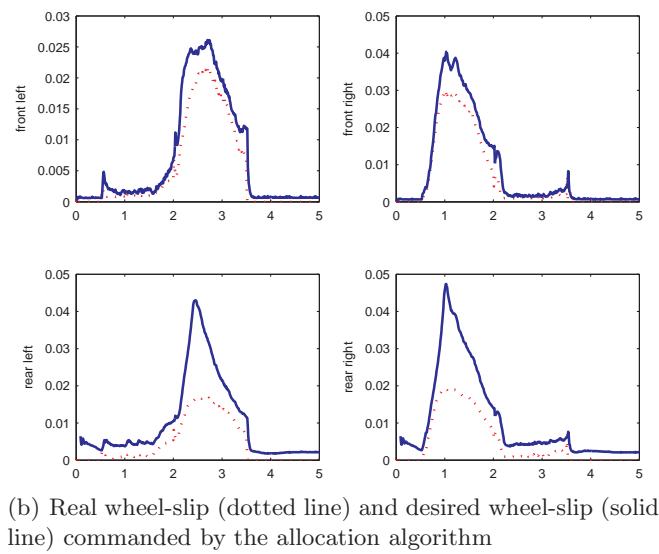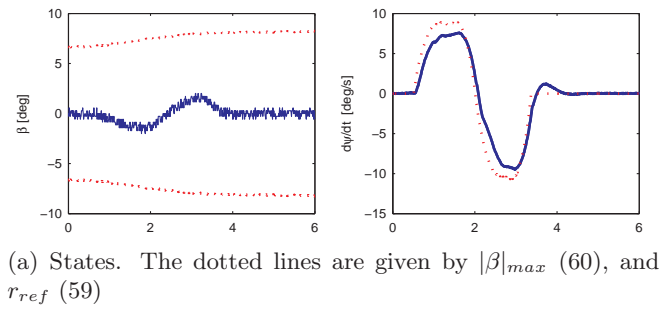
Figure 23: Simulation of the adaptive algorithm with a maximal tyre-road friction parameter initial guess $\hat{\mu}_H = 0.8$, while the real value is $\mu_H = 0.5$

Figure 24: Torque simulation of the adaptive algorithm with a maximal tyre-road friction parameter initial guess $\hat{\mu}_H = 0.8$, while the real value is $\mu_H = 0.5$
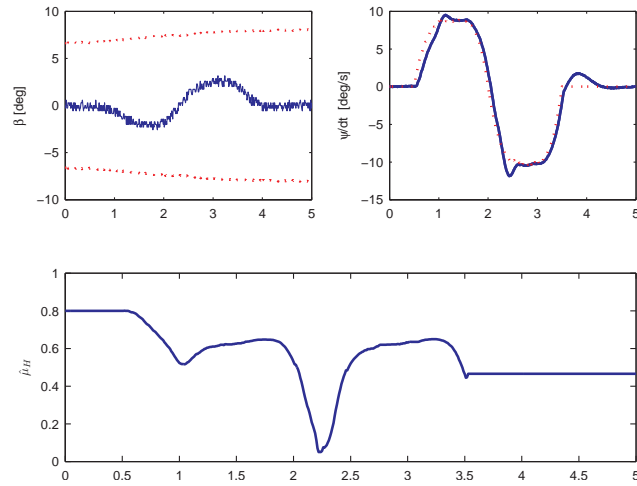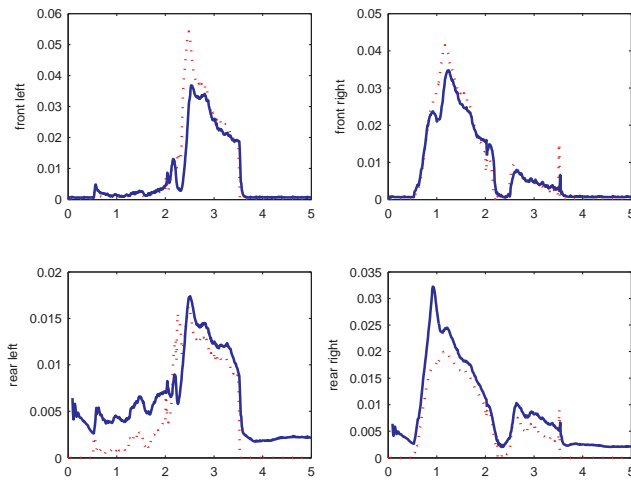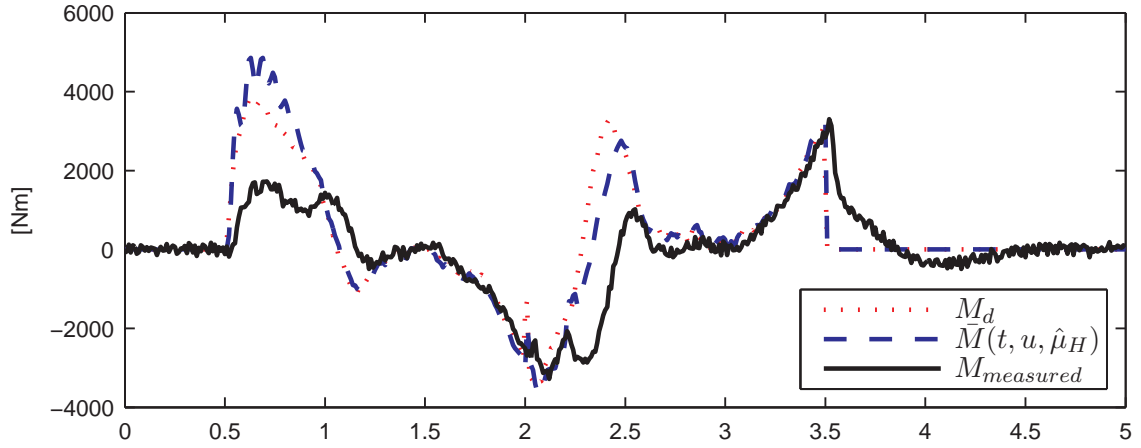
5 Control Design for Integrated Chassis Control (WP 2)

5.1 Introduction

5.1.1 Single-track model

We assume that the essential features of the lateral dynamic response of the vehicle to 4-wheel steering inputs can be captured using the *single-track model* [29]. In the single-track model, the two wheels at each axle are lumped into a single imaginary wheel located at the centre of the respective axle. The two resulting imaginary wheels are interconnected by a one-dimensional rigid element with the car's mass and moment of inertia around the vertical axis. Furthermore, we assume that the centre of gravity of the single-track model is at road level so that the roll, pitch and heave dynamics can be neglected. We also assume that the longitudinal speed is constant and that the only forces acting on the single-track model are cornering forces, i.e. horizontal forces perpendicular to the wheel plane generated by the interaction between the tyre and the road surface. Thus, the force acting on the front (respectively, rear) wheel of the single-track model corresponds to the combined cornering forces acting on both front (respectively, rear) wheels of the vehicle. The above assumptions amount to neglecting the influence of 4-wheel steering inputs on the longitudinal and vertical dynamics of the vehicle. Consequently, we focus on modelling how 4-wheel steering inputs affect the lateral dynamics of the single-track model. We consider that the lateral dynamic response of the single-track model to 4-wheel steering inputs is an acceptable approximation of the vehicle's lateral dynamic response to such inputs. Figure 25 depicts the single-track model subject to 4-wheel steering inputs, indicating the main elements necessary for the analysis of its lateral dynamic response to such inputs.

In Fig. 25, the set of reference axes *CG-xy*, with origin at the centre of gravity
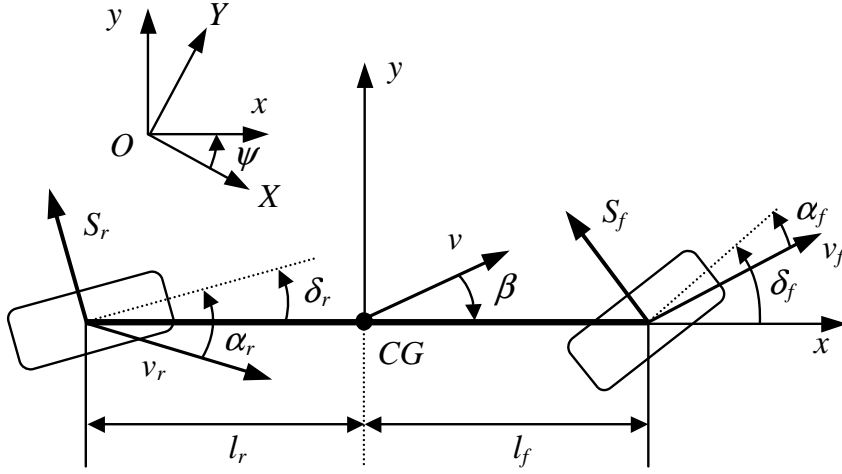
Figure 25: Single-track model of a 4-wheel steering car

CG, is fixed to the vehicle and O-XY is an inertial reference frame; l_f (respectively, l_r) is the distance from the centre of gravity to the front (respectively, rear) axle; v is the velocity of the vehicle with respect to O-XY; v_f (respectively, v_r) is the velocity at the front (respectively, rear) axle with respect to O-XY; ψ is the yaw angle and β is the sideslip angle. It is assumed that the front (respectively, rear) steering angle of the single-track model, δ_f (respectively, δ_r) in Fig. 25, is the steering angle of both front (respectively, rear) wheels of the vehicle. The force S_f (respectively, S_r) in Fig. 25 is the resultant of the combined cornering forces acting on the front (respectively, rear) axle. The angles α_f and α_r in Fig. 25 are the front and rear slip angles, respectively. The slip angle is the angular difference between the orientation of a wheel (the direction in which it is pointing) and the direction of its velocity (the direction in which it is travelling). The front slip angle α_f corresponds to the slip angle of the two front wheels of the vehicle while the rear slip angle α_r corresponds to the slip angle at the two rear wheels.

We base the design and analysis of the steering controller presented in this paper on a linear time-invariant system describing the single-track model's lateral dynamics at constant longitudinal speed under 4-wheel steering inputs. To obtain a state-space representation of such system, we apply the equations of motion of a rigid body to the single-track model under the assumptions introduced above together with the additional assumption of small front and rear steering angles. The latter assumption results in the angles β, α_f and α_r in Fig. 25 also being small. Proceeding as outlined above, we obtain the following differential equations governing sideslip and yaw rate:

$$\dot{\beta} = \dot{\psi} - \frac{S_f + S_r}{mv_x} \tag{83}$$

$$\ddot{\psi} = \frac{S_f l_f - S_r l_r}{I_{zz}} \tag{84}$$

where m is the mass of the vehicle, I_{zz} is its moment of inertia with respect to the vertical axis and v_x is the projection of the velocity vector along the $CG - x$ axis,

i.e. the vehicle longitudinal speed, which, for simplicity, we hereafter refer to as the vehicle speed. Since we assume it constant, the vehicle speed v_x can be considered as a parameter in equation (83).

5.1.2   Modelling of the cornering forces

When modelling the cornering forces, we consider the dynamics of the force generation at the tyres. Steering inputs do not produce cornering forces instanta-neously. Instead, the interaction between the tyre and the ground results in a gradual build-up of the cornering force. In other words, the cornering force generated by a tyre displays a transient response before reaching the steady-state value corresponding to a given steering input. When the slip angles are small, the tyres remain far from their adhesion limits and that steady-state value can be considered approximately proportional to the wheel slip angle. Regarding the transient response, we assume that it can be approximately described as a first order system whose input is the corresponding slip angle.

In addition to the tyre force dynamics, we consider the effect of the caster on the cornering forces generated by the front tyres, as it is assumed that the front steer-by-wire function is integrated with a conventional steering system. Conventional steering systems are designed so that the tyre-road contact patch trails behind the steering axis. This design feature is commonly referred to as the *caster trail* and results in a self-aligning torque on the front axle as a reaction to a front steering input. Considering the above, we model the total cornering force at the front axle follows:

$$\dot{S}_f = a \left(2C_T \left(\alpha_f - S_f \frac{n_s}{C_L} \right) - S_f \right) \tag{85}$$

where the parameter a, which depends on the vehicle speed, is the inverse of the time constant of the first order dynamics describing the tyre force generation; C_T is a constant describing the cornering stiffness of the tyres, n_s is a parameter related to the caster trail and C_L is an elasticity constant of the front steering system. We model the variation of the parameter a with the vehicle speed as follows:

$$a(v_x) = \frac{v_x}{a_1 v_x + a_2} \tag{86}$$

where a_1 and a_2 are parameters (a_1 is given in seconds and a_2 in meters). It can be seen in (85) that we model the effect of the self-aligning torque generated by the caster trail as a dynamic reduction in the effective slip angle at the front wheels.

Since it is assumed that each rear wheel is turned individually by an electro-hydraulic actuator, there is no caster trail at the rear axle. Thus, we model the total cornering force generated at the rear axle as follows:

$$\dot{S}_r = a \left(2C_T \alpha_r - S_r \right) \tag{87}$$

Considering the geometry of the single-track model and its kinematics as a rigid

body, the following expressions for α_f and α_r are obtained assuming small angles:

$$\alpha_f = \delta_f + \beta - \frac{l_f}{v_x}\dot{\psi} \tag{88}$$

$$\alpha_r = \delta_r + \beta + \frac{l_r}{v_x}\dot{\psi} \tag{89}$$

Substituting (88) into (85) and (89) into (87) we obtain the following equations relating the front and rear cornering forces to δ_f and δ_r, respectively:

$$\dot{S}_f = a\left(2C_T\left(\delta_f - S_f\frac{n_s}{C_L} + \beta - \frac{l_f\dot{\psi}}{v_x}\right) - S_f\right) \tag{90}$$

$$\dot{S}_r = a\left(2C_T\left(\delta_r + \beta + \frac{l_r\dot{\psi}}{v_x}\right) - S_r\right) \tag{91}$$

5.1.3   Modelling of the steering actuators

We model front and rear steering actuators as second order systems. The input to the front steering actuator is denoted as δ_f^i, and the output is the actual angle by which the two front wheels are turned, δ_f. We do not take into account the effect of the Ackermann steering geometry ([30] [31]), which makes possible for the outside wheel to have a smaller turning angle than the inside one when negotiating a corner. Both rear steering actuators are modelled as a single second order system whose input is denoted as δ_r^i, and whose output is the turning angle of both rear wheels, δ_r. Thus, the actuator models are of the following form:

$$\begin{bmatrix} \dot{\delta}_f \\ \ddot{\delta}_f \end{bmatrix} = \begin{bmatrix} A_{11}^f & A_{12}^f \\ A_{21}^f & A_{21}^f \end{bmatrix} \begin{bmatrix} \delta_f \\ \dot{\delta}_f \end{bmatrix} + \begin{bmatrix} b_1^f \\ b_2^f \end{bmatrix} \delta_f^i \tag{92}$$

$$\begin{bmatrix} \dot{\delta}_r \\ \ddot{\delta}_r \end{bmatrix} = \begin{bmatrix} A_{11}^r & A_{12}^r \\ A_{21}^r & A_{21}^r \end{bmatrix} \begin{bmatrix} \delta_r \\ \dot{\delta}_r \end{bmatrix} + \begin{bmatrix} b_1^r \\ b_2^r \end{bmatrix} \delta_r^i \tag{93}$$

The second order transfer functions corresponding to the state-space models above are given by:

$$\delta_f(s) = \frac{1}{(\frac{1}{f_f})^2 s^2 + 2(\frac{d_f}{f_f})s + 1}\delta_f^i(s) \tag{94}$$

$$\delta_r(s) = \frac{1}{(\frac{1}{f_r})^2 s^2 + 2(\frac{d_r}{f_r})s + 1}\delta_r^i(s) \tag{95}$$

5.1.4   State-space representation of the system

Considering the above, we can model the lateral dynamics of a vehicle travelling at a given fixed longitudinal speed and subject to 4-wheel steering inputs as a linear time-invariant system with two inputs (δ_f^c and δ_r^c) and two outputs (β and $\dot{\psi}$). We include

below the 8th order state-space representation of such system. This representation is obtained by combining equations (83), (84), (90), (91), (5.1.3) and (5.1.3).

$$\dot{x} = Ax + Bu^i \tag{96}$$

$$y = Cx + Du^i \tag{97}$$

where

$$u^c = \begin{bmatrix} \delta_f^i \\ \delta_r^i \end{bmatrix}, \quad y = \begin{bmatrix} \beta \\ \dot{\psi} \end{bmatrix}, \quad x = \begin{bmatrix} \beta \\ \dot{\psi} \\ S_f \\ S_r \\ \delta_f \\ \dot{\delta}_f \\ \delta_r \\ \dot{\delta}_r \end{bmatrix}, \tag{98}$$

$$A = \begin{bmatrix}
0 & 1 & -\frac{1}{mv_x} & -\frac{1}{mv_x} & 0 & 0 & 0 & 0 \\
0 & 0 & \frac{l_f}{I_{zz}} & -\frac{l_r}{I_{zz}} & 0 & 0 & 0 & 0 \\
2aC_T & -\frac{2aC_T l_f}{v_x} & -a(1 + 2C_T \frac{n_s}{C_L}) & 0 & 2aC_T & 0 & 0 & 0 \\
2aC_T & \frac{2aC_T l_r}{v_x} & 0 & -a & 0 & 0 & 2aC_T & 0 \\
0 & 0 & 0 & 0 & A_{11}^f & A_{12}^f & 0 & 0 \\
0 & 0 & 0 & 0 & A_{21}^f & A_{22}^f & 0 & 0 \\
0 & 0 & 0 & 0 & 0 & 0 & A_{11}^r & A_{12}^r \\
0 & 0 & 0 & 0 & 0 & 0 & A_{21}^r & A_{22}^r
\end{bmatrix} \tag{99}$$

$$B = \begin{bmatrix} 0 & 0 \\ 0 & 0 \\ 0 & 0 \\ 0 & 0 \\ b_1^f & 0 \\ b_2^f & 0 \\ 0 & b_1^r \\ 0 & b_2^r \end{bmatrix}, \quad C = \begin{bmatrix} 1 & 0 & 0 & 0 & 0 & 0 & 0 & 0 \\ 0 & 1 & 0 & 0 & 0 & 0 & 0 & 0 \end{bmatrix} \quad \text{and} \quad D = \begin{bmatrix} 0 & 0 \\ 0 & 0 \end{bmatrix} \tag{100}$$

As indicated above, the vehicle speed v_x is considered as a parameter in the model.

5.1.5   Input-output representation and communication delay

We intend to use the simplified model of the vehicle lateral dynamics introduced above as the basis for the linear analysis and design of the steering controller. Since we will adopt a frequency domain approach to linear analysis and design, we will make extensive use of the transfer matrix function corresponding to the steady-state representation (96)-(97). For a given fixed vehicle speed, that matrix transfer function is given by:

$$G'(s) = C(sI - A)^{-1}B + D = \begin{bmatrix} g_{11}'(s) & g_{12}'(s) \\ g_{21}'(s) & g_{22}'(s) \end{bmatrix} \tag{101}$$
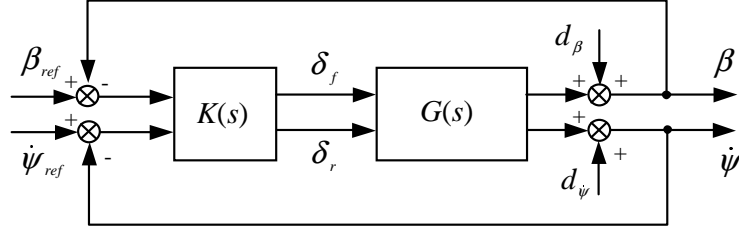
Figure 26: Design of a linear multivariable steering controller for fixed vehicle speed

The matrix transfer function (101) relates the input to the steering actuators to the outputs in the Laplace domain:

$$\left[\begin{array}{c} \beta(s) \\ \dot{\psi}(s) \end{array} \right] = G'(s) \left[\begin{array}{c} \delta_f^i(s) \\ \delta_r^i(s) \end{array} \right] \tag{102}$$

As we stated above, the steer-by-wire system is characterised by a communication delay between the controller's output and the steering actuator's input. The matrix transfer representation above allows for the straightforward modelling of that communication delay as a pure time delay of τ seconds. We can express the system response to the steering angles demanded by the controller, which we denote as δ_f^c and δ_r^c, as follows:

$$\left[\begin{array}{c} \beta(s) \\ \dot{\psi}(s) \end{array} \right] = G(s) \left[\begin{array}{c} \delta_f^c(s) \\ \delta_r^c(s) \end{array} \right] \tag{103}$$

where the matrix transfer function $G(s)$ is given by:

$$G(s) = \left[\begin{array}{cc} g_{11}(s) & g_{12}(s) \\ g_{21}(s) & g_{22}(s) \end{array} \right] = G'(s) \left[\begin{array}{cc} e^{-\tau s} & 0 \\ 0 & e^{-\tau s} \end{array} \right] = \left[\begin{array}{cc} g'_{11}(s)e^{-\tau s} & g'_{12}(s)e^{-\tau s} \\ g'_{21}(s)e^{-\tau s} & g'_{22}(s)e^{-\tau s} \end{array} \right] \tag{104}$$

We use a Padè rational approximation of the function $e^{-\tau s}$ to facilitate the plotting of the system's frequency response.

5.2 Multivariable control design problem

We use the 2-by-2 matrix transfer function $G(s)$ in (104) as the basis for the design of steering controllers valid for different constant vehicle speeds. To design a controller, we solve the classical 2-by-2 linear multivariable control design problem depicted in Fig. 26.

The use of a linear model of the vehicle lateral dynamics is justified by the fact that, in principle, our objective is to design controllers to track reference signals corresponding to typical driver's inputs during "normal" driving. These inputs can be assumed to result in small steering and slip angles, with the tyres remaining far from their adhesion limits. Although a linear controller $K(s)$ designed based on a given $G(s)$ is only valid for the corresponding vehicle speed, a set of local controllers designed for different vehicle speeds can be combined using gain-scheduling techniques into a non-linear controller valid across the desired speed envelope.

5.3 Control specifications

The main requirements for the controlled 4-wheel steering car are summarised below:

1. Tracking sideslip and yaw rate reference signals with the highest possible closed-loop bandwidth. These reference signals are obtained in real-time from the driver's inputs to the steering wheel and pedals.

2. Rejecting any disturbances in sideslip and yaw rate with the highest possible bandwidth, so that their interference with the driver's actions is minimised.

3. Maintaining tracking and disturbance rejection performance for vehicle speeds between 10 and 60 m/s and for driving situations involving speed changes, such as acceleration and braking.

4. Robustness with respect to uncertainty in the vehicle model, in particular with respect to changes in the effective tyre stiffness under different road conditions.

5. Stability and satisfactory degraded performance in the event of saturation of the rear actuators. We require the system to remain stable and the controller to be able to at least track the reference yaw rate signal with an acceptable degree of accuracy.

6. Integrity with respect to loop or rear actuator failure. The system must remain stable should either of these failure modes occur. In addition, the controller must retain full control of the yaw rate in the event of rear actuator failure.

5.3.1 Individual Channel Design (ICD) methodology

ICD is a frequency-domain approach to the analysis and design of linear time-invariant multivariable control systems. The detailed theoretical derivation and justification of the ICD methodology for 2-by-2 systems was laid out in [32]. The generalisation of the methodology for m-by-m systems can be found in [33]. ICD provides a solid framework for the application of concepts and techniques from classical linear SISO control, such as Nyquist and Bode plots and gain and phase margins, to multivariable control design problems. The ICD approach is application-oriented and involves an interplay between control specifications, plant uncertainty and the control synthesis process itself. One of its main features is that it allows one to explore the potential and limitations of diagonal feedback control for a given system. According to the ICD methodology, an m-input, m-output feedback control system with a diagonal controller can be decomposed, without any loss of information, into m equivalents SISO feedback control systems called *channels*. Each individual channel originates from the pairing of a plant output to its corresponding reference input. Consequently, a channel has its own performance specifications expressed in terms of its response to the reference input. Each channel comprises a single feedback loop and a compensator, which must be designed to meet the channel specifications. According to ICD, the multivariable control problem in Figure 26 can be decomposed into the two channels shown in Figure 27.
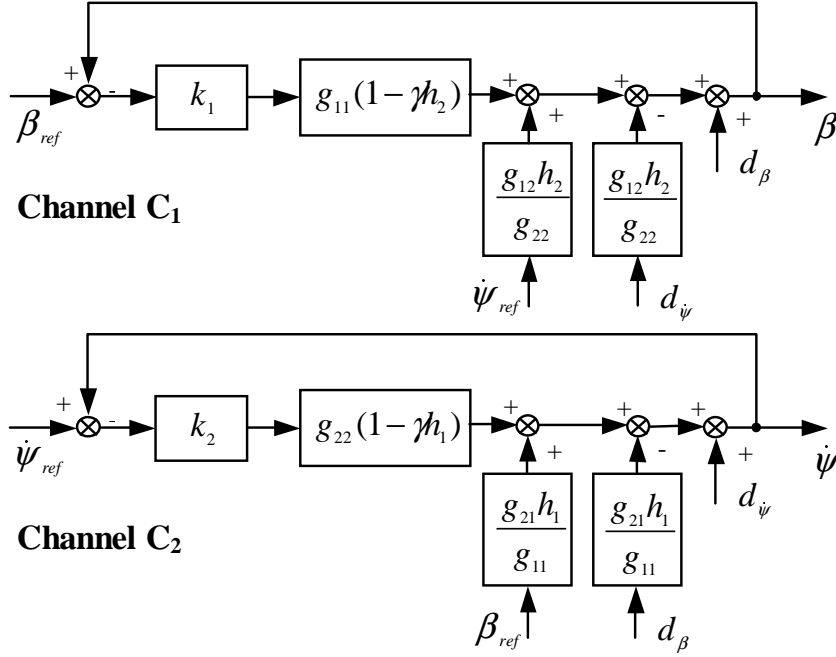
Figure 27: Channel decomposition of the multivariable control design problem according to ICD

Channel C_1 has the open-loop transmittance

$$c_1(s) = k_1(s)g_{11}(s)(1 - \gamma(s)h_2(s)) \tag{105}$$

where

$$\gamma(s) = \frac{g_{12}(s)g_{21}(s)}{g_{11}(s)g_{22}(s)} \tag{106}$$

and

$$h_2(s) = \frac{k_2(s)g_{22}(s)}{1 + k_2(s)g_{22}(s)} \tag{107}$$

and is subject to the additive disturbance $d_\beta(s)$. Channel C_2 has the open-loop transmittance

$$c_2(s) = k_2(s)g_{22}(s)(1 - \gamma(s)h_1(s)) \tag{108}$$

where

$$h_1(s) = \frac{k_1(s)g_{11}(s)}{1 + k_1(s)g_{11}(s)} \tag{109}$$

and is subject to the additive disturbance $d_{\dot\psi}(s)$. The effect of $\dot\psi_{ref}(s)$ and $d_{\dot\psi}(s)$ on channel C_1 is taken into account through the additive disturbances

$$\frac{g_{12}(s)}{g_{22}(s)}h_2(s)\dot\psi_{ref}(s) \quad \text{and} \quad -\frac{g_{12}(s)}{g_{22}(s)}h_2(s)d_{\dot\psi}(s) \tag{110}$$

Table 7: Open-loop channel poles and zeros.

	Zeros	Poles
Channel C_1	Zeros of $(1 - \gamma h_2)$	Poles of $g_{11}, g_{12}, g_{21}, h_2$
Channel C_2	Zeros of $(1 - \gamma h_1)$	Poles of $g_{22}, g_{12}, g_{21}, h_1$

Analogously, the effect of $\dot{\beta}_{ref}(s)$ and $d_\beta(s)$ on channel C_2 is taken into account through the additive disturbances

$$\frac{g_{21}(s)}{g_{11}(s)}h_1(s)\beta_{ref}(s) \quad \text{and} \quad -\frac{g_{21}(s)}{g_{11}(s)}h_1(s)d_\beta(s) \tag{111}$$

The closed-loop response of the channels are given by:

$$\beta(s) = t_{11}(s)\beta_{ref}(s) + t_{12}(s)\dot{\psi}_{ref}(s) + s_{11}(s)d_\beta(s) + s_{12}(s)d_{\dot{\psi}}(s) \tag{112}$$

$$\dot{\psi}(s) = t_{21}(s)\beta_{ref}(s) + t_{22}(s)\dot{\psi}_{ref}(s) + s_{21}(s)d_\beta(s) + s_{22}(s)d_{\dot{\psi}}(s) \tag{113}$$

where

$$t_{ii}(s) = \frac{c_i(s)}{1 + c_i(s)}, \quad i = 1, 2 \tag{114}$$

$$t_{ij}(s) = \frac{g_{ij}(s)h_j(s)}{g_{jj}(s)}\frac{1}{1 + c_i(s)}, \quad i = 1, 2; \; j = 1, 2; \; i \neq j \tag{115}$$

$$s_{ii}(s) = \frac{1}{1 + c_i(s)}, \quad i = 1, 2 \tag{116}$$

$$s_{ij}(s) = -t_{ij}(s), \quad i = 1, 2; \; j = 1, 2; \; i \neq j \tag{117}$$

Providing that there are no pole-zero cancellations, the pole-zero structure of the open-loop channel transmittances, c_1 and c_2, is given in Table 7

The robust stability of the multivariable control system is equivalent to the robust stability of the channels providing that the Nyquist plots of the two multivariable structure functions $\gamma(s)h_j(s)$ for $j = 1, 2$ remain far from the (1,0) point (add reference).

5.4 Preliminary analysis according to ICAD

In this section, we analyse the matrix transfer function $G(s)$ obtained by setting the values of the model parameters to those corresponding to a Mercedes A-Class, which is the vehicle used to test the steering controller. The analysis is carried out according to the ICD framework and aims to identify potential difficulties in the design of linear controllers $K(s)$ for different vehicle speeds. Figure 28 shows the Bode diagrams of the resulting frequency responses.

The matrix transfer function is stable for the speeds considered, as it has no right half-plane poles (RHPPs). All the elements of the matrix transfer function are also stable for those speeds. While the elements $g_{12}(s)$, $g_{21}(s)$ and $g_{22}(s)$ are minimum phase, the element $g_{11}(s)$ has one real right half-plane zero (RHPZ), the frequency of which increases with speed. Figure 29 shows the Nyquist and Bode
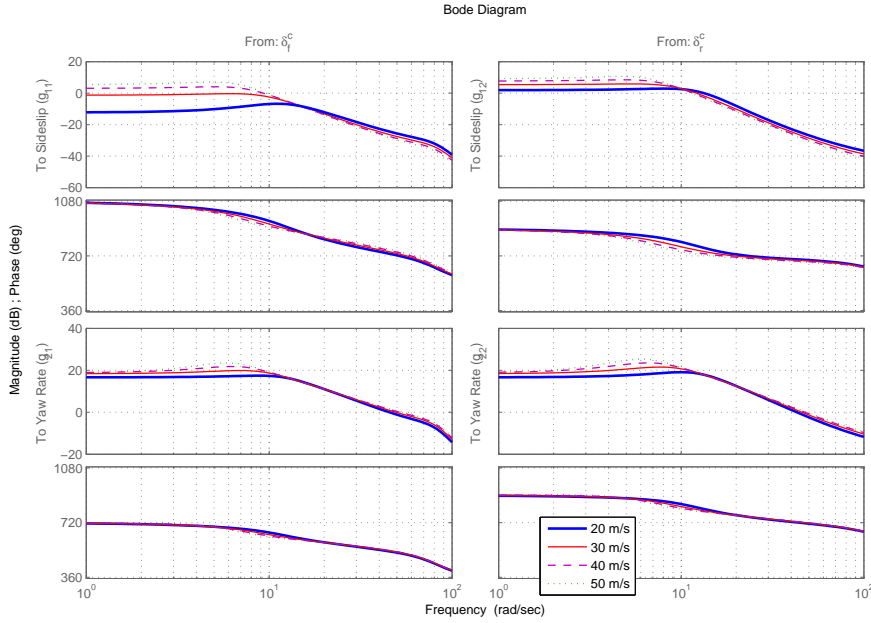
Figure 28: Bode plots of $G(s)$ for different vehicle speeds

plots of the corresponding multivariable structure function $\gamma(s)$ for the different vehicle speeds considered. This function is not only a measure of the strength of the cross-coupling (when its magnitude is low, the interaction between the channel signals is low; otherwise, the interaction is high), it also gives information about the achievable channel performance and the potential robustness of the design. The function $\gamma(s)$ has one RHPP, which is the RHPZ in $g_{11}(s)$. Since the Nyquist plot of $\gamma(s)$ encircles the point (1,0) once in the anti-clockwise direction (see Fig. 29), the function $(1 - \gamma(s))$ does not have any RHPZs and the system is minimum phase. It can also be observed in Fig. 29 that the limit of $\gamma(s)$ as s tends to $+\infty$ is less than one for the speeds considered. Consequently, according to [[34]], the achievement of high-performance control (bandwidth in both channels greater than the frequency of any significant system dynamics) using stable and minimum-phase controllers is not hampered by the structure of the plant.

The RHPZ in $g_{11}(s)$ plays an important role in the potential integrity of the system to feedback loop failure [[35]]. In order to guarantee the stability of the system under loop failure, e.g. when a sensor breaks and no measurement is fed back to the controller, the open-loop transmittances of both channels must be stable. Thus, according to Table 7, all the individual elements of the matrix transfer function as well as both $h_1(s)$ and $h_2(s)$ must be stable. However, according to [34], a necessary condition to ensure that the channels are minimum-phase (and therefore high-performance control is possible) when $\lim_{s \to +\infty} \gamma(s) < 1$ is that $h_i(s)$ has the same number of RHPPs as $g_{ii}(s)$ has RHPZs, with i=1, 2. This condition ensures that $\gamma(s)h_i(s)$ and $\gamma(s)$ have the same structure. Then, the RHPZ in $g_{11}(s)$ results
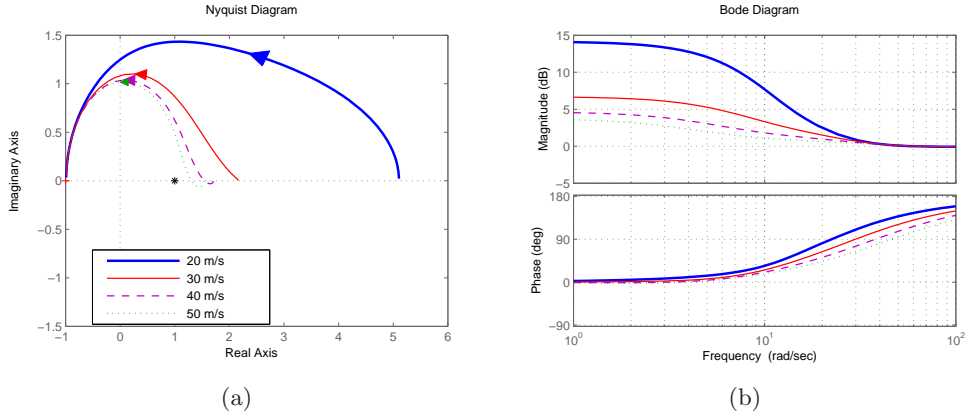
Figure 29: Nyquist plot and Bode diagram of $\gamma(s)$ for different vehicle speeds

in a RHPP in $h_1(s)$. Consequently, integrity to loop failure cannot be achieved unless the requirement for high-performance control is relaxed by allowing one of the channels to be non-minimum phase and adequately limiting its bandwidth. Another possibility is to swap the current assignment of inputs to outputs (from δ_f^c to $\dot{\psi}$ instead of β and from δ_r^c to β instead of $\dot{\psi}$) to take advantage of the fact that the transfer functions $g_{12}(s)$ and $g_{21}(s)$, which would be the diagonal elements of the resulting matrix transfer function, are minimum-phase. Hence, swapping the assignment of inputs to outputs can in principle facilitate the attainment of both integrity to loop failure and high-performance control.

As it is the case in SISO control, the gain and phase margins of the channel's transmittance $c_i(s)$ obtained for a given controller $k_i(s)$ are indicators of the channel's performance. In addition, those margins are also measures of the robustness of the closed-loop system with respect to unstructured uncertainty in the elements of the transfer function matrix if the Nyquist plot of the function $\gamma(s)h_i(s)$ with $i=1,\,2$ does not go near the point (1,0) except for frequencies significantly higher that the gain crossover frequency of the corresponding channel. If the Nyquist plot of $\gamma(s)h_i(s)$ goes near the point (1,0) at frequencies close or below the channel gain crossover frequency, then the relative uncertainty in $(1-\gamma(s)h_i(s)$, and consequently of the open-loop transmittance, is much larger than the relative uncertainty in $g_{ii}(s)$ and $\gamma(s)h_i(s)$. In such a situation, traditionally satisfactory phase and gain margins for the channels do not guarantee a worthwhile degree of robustness. As it can be seen in Fig. 29, for high vehicle speed the multivariable structure function $\gamma(s)$ goes near the point (1,0) at low frequencies for high vehicle speed. This proximity to the point (1,0) indicates that the robustness of the system may be compromised unless the bandwidth of at least one of the channels is kept low for high vehicle speeds. If the bandwidth of both channels were high, then the gain of both would be high up to a a high frequency value and the gain of both $h_1(s)$ and $h_2(s)$ would be approximately one up to that frequency. Consequently, both $\gamma(s)h_1(s)$ and $\gamma(s)h_2(s)$ would get near (1,0) at frequencies close or below cross-over. On the other hand,

if the bandwidth of one of the channels, say C_1, is kept sufficiently low so that the roll-off in $h_1(s)$ at low frequencies prevents $\gamma(s)h_1(s)$ from going near $(1,0)$, then the gain and phase margins of C_2 are true measures of robustness. And even though $\gamma(s)h_2(s)$ would still get near $(1,0)$, it would do so at frequencies higher than the crossover frequency of C_1, and hence its gain and phase margins would also be true measures of robustness.

An analysis of the elements of the matrix transfer function reveals that

$$\left| \frac{g_{21}(s)}{g_{11}(s)} \right| \gg 1 \gg \left| \frac{g_{12}(s)}{g_{22}(s)} \right| \tag{118}$$

Even though the magnitudes $\left| \frac{g_{21}(s)}{g_{11}(s)} \right|$ and $\left| \frac{g_{12}(s)}{g_{22}(s)} \right|$ depend on the units in which the signals are expressed, it can then be concluded that at least one of the two will always be larger than one for the frequencies of interest, as their product $|\gamma(s)|$, which is dimensionless, is larger than 1 (see Figure 29). In the context at hand, the large magnitude of $\left| \frac{g_{21}(s)}{g_{11}(s)} \right|$ can hamper the disturbance rejection performance of channel C_2, as it would contribute to amplify the disturbances affecting channel C_2 through channel cross-coupling $(\frac{g_{21}(s)}{g_{11}(s)} h_1(s) \beta_{ref}(s)$ and $-\frac{g_{21}(s)}{g_{11}(s)} h_1(s) d_\beta(s))$.

The discussion above highlights some potential difficulties in the design of the linear controllers $k_1(s)$ and $k_2(s)$ for fixed vehicle speeds. Assuming that satisfactory linear controllers are designed for a series of vehicle speeds, it would still be necessary to use gain-scheduling techniques to combined those linear controllers into a non-linear controller valid within the desired speed range and capable of operating with varying speed. In view of the significant differences in the dynamic response of the system across the speed range considered (see Figure 28), this task may not be trivial.

5.4.1 Ideal model of the dynamic response of the vehicle to 4-wheel steering inputs

As discussed in the previous section, the design of a diagonal controller valid within the desired speed range and with satisfactory disturbance rejection performance poses potential difficulties. To avoid these difficulties, we propose to express the control design problem in terms of a virtual plant that results from pre-compensating the original plant $G(s)$ and introducing a speed-dependent inner loop. This will result in an augmented plant, denoted as $\tilde{G}(s)$, which will serve as the basis for the design. We will show that controlling the augmented plant is a much simpler problem than controlling the original plant directly and that the resulting steering controller displays satisfactory robustness and performance within the desired speed range.

The pre-compensator and the inner speed-dependent feedback loop mentioned above constitute what we will refer to from now on as the structure of the steering controller. These two elements aim to mitigate the effects of the unbalance in the plant and to facilitate the design process for different vehicle speeds. We intend to design the two elements based on an ideal model of 4-wheel steering dynamics. The objective of augmenting the plant according to the basic physics of 4-wheel steering

is to obtain a partially decoupled, nearly speed-invariant augmented plant for which the design of a diagonal controller is straightforward. We now introduce the ideal model of the vehicle lateral dynamics under 4-wheel steering inputs that we intend to use as the foundation for the design of the structure of the steering controller. The model is a simplified version of the model introduced above in section 5.1.5.

For small values of α_f and α_r and disregarding the dynamics of the tyre force generation, the forces S_f and S_r can be approximated by the following expressions: [31]:

$$S_f = K_f \alpha_f \tag{119}$$
$$S_r = K_r \alpha_r \tag{120}$$

The constant K_f in (119) can be written as twice the result of adequately reducing the cornering stiffness to take into account the caster effect:

$$K_f = 2\frac{C_T}{1 + 2C_T\frac{n_s}{C_L}} \tag{121}$$

Since no caster effect is generated at the rear axle, the constant K_r in (120) is simply twice the cornering stiffness:

$$K_r = 2C_T \tag{122}$$

Equations (83), (84), (88), (89), (119) and (120) can be combined into the state-space representation of a linear time-invariant system with two inputs (δ_f and δ_r) and two outputs (β and $\dot{\psi}$). The resulting state-space representation is given below:

$$\dot{x}^i = A^i x^i + B^i u^i \tag{123}$$
$$y^i = C^i x^i + D^i u^i \tag{124}$$

where

$$u^i = \begin{bmatrix} \delta_f \\ \delta_r \end{bmatrix}, \quad y^i = x^i = \begin{bmatrix} \beta \\ \dot{\psi} \end{bmatrix}, \tag{125}$$

$$A^i = \begin{bmatrix} -\dfrac{K_f + K_r}{mv_x} & \dfrac{K_f l_f - K_r l_r}{mv_x^2} + 1 \\[2ex] \dfrac{K_f l_f - K_r l_r}{I_{zz}} & -\dfrac{K_f l_f^2 + K_r l_r^2}{I_{zz}v_x} \end{bmatrix}, \quad B^i = \begin{bmatrix} -\dfrac{K_f}{mv_x} & -\dfrac{K_r}{mv_x} \\[2ex] \dfrac{K_f l_f}{I_{zz}} & -\dfrac{K_r l_r}{I_{zz}} \end{bmatrix}, \tag{126}$$

$$C^i = \begin{bmatrix} 1 & 0 \\ 0 & 1 \end{bmatrix} \quad \text{and} \quad D^i = \begin{bmatrix} 0 & 0 \\ 0 & 0 \end{bmatrix} \tag{127}$$

The matrix transfer function of the system with the state-representation (123)-(124) is given by

$$G^i(s) = C^i(sI - A^i)^{-1}B^i + D^i = \begin{bmatrix} g_{11}^i(s) & g_{12}^i(s) \\ g_{21}^i(s) & g_{22}^i(s) \end{bmatrix} \tag{128}$$

The matrix transfer function (101) relates the front and rear steering angles to the outputs in the Laplace domain:

$$\left[\begin{array}{c} \beta(s) \\ \dot{\psi}(s) \end{array} \right] = G^i(s) \left[\begin{array}{c} \delta_f(s) \\ \delta_r(s) \end{array} \right] \tag{129}$$

The ideal model introduced above describes the linearised lateral dynamics of the single-track model under front and rear steering around a nominal trajectory given by zero sideslip, zero yaw rate, zero steering angles and constant vehicle speed. Neither the tyre force generation dynamics nor the steering actuators are considered in the model, which relies on simple linear approximations of the cornering forces.

5.5   Structure of the steering controller

In order to simplify the design process, we take a different approach and state the control design problem in terms of the virtual plant that results from pre-compensating $G(s)$ with a constant matrix gain, i.e. linearly transforming the inputs, and then introducing a speed-dependent matrix gain in a feedback path around the pre-compensated plant. By modifying $G(s)$ in this manner and basing the design on the resulting virtual plant, we impose a structure that facilitates the design of a diagonal controller valid for varying vehicle speed. This is due to the fact that the virtual plant to be controlled, which we denote as $\tilde{G}(s)$, yields a nearly speed-invariant yaw rate response to one of the transformed inputs and is virtually decoupled from the other one. The derivation of the controller structure is explained in detail below based on the ideal model of 4-wheel steering dynamics introduced in the previous section.

Linear input transformation Suppose that the inputs to the plant $G^i(s)$ are the result of the following linear transformation:

$$\left[\begin{array}{c} \delta_f \\ \delta_r \end{array} \right] = E \left[\begin{array}{c} \Delta_1 \\ \Delta_2 \end{array} \right] \tag{130}$$

where $\mathrm{E} \in \Re^{2x2}$. Considering (130), the resulting dynamical equation for the single-track model with respect to the new inputs is:

$$\dot{x}^i = A^i x^i + B^i E \Delta = A^i x^i + B_1^i \Delta, \quad \text{with} \quad \Delta = \left[\begin{array}{c} \Delta_1 \\ \Delta_2 \end{array} \right] \tag{131}$$

If we choose

$$E = -\frac{1}{\frac{K_r}{K_f}\left(1 + \frac{l_r}{l_f}\right)} \left[\begin{array}{cc} \dfrac{K_r l_r}{K_f l_f} & -\dfrac{K_r}{K_f} \\ -1 & -1 \end{array} \right] \tag{132}$$

the resulting matrix B_1^i is diagonal:

$$B_1^i = \left[\begin{array}{cc} -\dfrac{K_f}{m v_x} & 0 \\ 0 & \dfrac{K_f K_f}{I_{zz}} \end{array} \right] \tag{133}$$

The chosen matrix E results in the following transformed inputs:

$$\Delta_1 = \delta_f + \frac{K_r}{K_f}\delta_r \tag{134}$$

$$\Delta_2 = \delta_f - \frac{K_r l_r}{K_f l_f}\delta_r \tag{135}$$

A physical interpretation of these new inputs is in terms of a mode given by Δ_1, which excites the sideslip by steering front and rear wheels in the same direction, and a mode given by Δ_2, which excites the yaw rate by steering front and rear wheels in opposite directions. It can be argued that by using Δ_1 and Δ_2 as control actions the 4-wheel steering vehicle is controlled in a "natural" way, separating the dynamics into their linear and rotational components. The resulting dynamical equation of the yaw rate with respect to the new inputs is:

$$\frac{I_{zz}}{K_f l_f}\ddot{\psi} + \frac{K_f l_f^2 + K_r l_r^2}{K_f l_f v_x}\dot{\psi} = \Delta_2 + \left(1 - \frac{K_r l_r}{K_f l_f}\right)\beta \tag{136}$$

Taking Laplace transforms of both sides of equation (136) and rearranging results in:

$$\dot{\psi}(s) = \frac{K_1}{s + p(v_x)}\Delta_2(s) + \frac{K_1 K_2}{s + p(v_x)}\beta(s) \tag{137}$$

where

$$K_1 = \frac{K_f l_f}{I_{zz}}, \quad K_2 = 1 - \frac{K_r l_r}{K_f l_f}, \quad \text{and} \quad p(v_x) = \frac{K_f l_f^2 + K_r l_r^2}{I_{zz} v_x} \tag{138}$$

The yaw rate dynamics are characterised by a speed-varying first order pole at frequency $p(v_x)$ and are coupled with the sideslip dynamics. **Speed-dependent feedback element** We now introduce a feedback element of the form:

$$\Delta = \tilde{\Delta} - Fy \tag{139}$$

which results in the new vector of controllable inputs $\tilde{\Delta} = \begin{bmatrix} \tilde{\Delta}_1 \\ \tilde{\Delta}_2 \end{bmatrix}$. The matrix $F \in \Re^{2x2}$ is given by

$$F = \begin{bmatrix} 0 & 0 \\ K_2 & K_v(v_x) \end{bmatrix} \tag{140}$$

with K_2 from (138) and $K_v(v_x)$ defined as

$$K_v(v_x) = K_0 - \frac{p(v_x)}{K_1} \tag{141}$$

with K_1 from (138) and K_0 an arbitrary constant. Since $y^i = x^i$, the state-space equation can be written as follows:

$$\dot{x}^i = A^i x^i + B_1^i(\tilde{\Delta} - Fx^i) = (A^i - B_1^i F)x^i + B_1^i \tilde{\Delta} \tag{142}$$

where

$$\tilde{A}^i = A^i - B_1^i F = \begin{bmatrix} -\dfrac{K_f + K_r}{mv_x} & \dfrac{K_f l_f - K_r l_r}{mv_x^2} + 1 \\[3ex] 0 & -\dfrac{K_0 K_f l_f}{I_{zz}} \end{bmatrix} \tag{143}$$

The corresponding matrix transfer function with respect to the new controllable inputs is upper-triangular:

$$\tilde{G}^i(s) = C^i(sI - \tilde{A}^i)^{-1} B_1^i + D^i = \begin{bmatrix} \tilde{g}_{11}^i(s) & \tilde{g}_{12}^i(s) \\ 0 & \tilde{g}_{22}^i(s) \end{bmatrix} \tag{144}$$

The resulting dynamical equation of the yaw rate with respect to the new controllable inputs $\tilde{\Delta}_1$ and $\tilde{\Delta}_2$ is speed-invariant, taking the form:

$$\ddot{\psi} = -K_0 K_1 \dot{\psi} + K_1 \tilde{\Delta}_2 \tag{145}$$

We choose K_0 to be:

$$K_0 = \frac{K_f l_f^2 + K_r l_r^2}{K_f l_f v_{x0}} \tag{146}$$

with v_{x0} an arbitrary fixed vehicle speed. Then, taking Laplace transforms of both sides of (145) results in:

$$\dot{\psi}(s) = \frac{K_1}{s + p(v_{x0})} \tilde{\Delta}_2 \tag{147}$$

The introduction of the feedback element described above results in the yaw rate dynamics depending only on one of the two inputs to be controlled, $\tilde{\Delta}_2$. Besides, the yaw rate response to it is speed-invariant and characterised by a fixed first order pole at frequency $p(v_{x0})$.

The resulting dynamical equation of the sideslip with respect to the new controllable inputs $\tilde{\Delta}_1$ and $\tilde{\Delta}_2$ takes the following form:

$$\dot{\beta} = -\frac{K_f + K_r}{mv_x}\beta + \left(1 + \frac{K_f l_f - K_r l_r}{mv_x^2}\right)\dot{\psi} - \frac{K_f}{mv_x}\tilde{\Delta}_1 \tag{148}$$

5.6   Control design

Augmented plant $\tilde{G}(s)$ Considering the above, we base the control design on the virtual plant $\tilde{G}(s)$ that results from pre-compensating $G(s)$ with the constant matrix E and subsequently introducing the speed-dependent feedback element F. Since we intend to apply the ICD design methodology , we assume that $\tilde{G}(s)$ is to be controlled by a diagonal controller. Consequently, the multivariable control problem in Figure 26 can be restated as shown in Figure 30, which depicts the proposed controller structure.

Figure 31 shows the Bode plots of the elements of the transfer function $\tilde{G}(s)$ for different vehicle speeds. Again, the values of the model parameters are those corresponding to a Mercedes S Class. The values of the parameters of the controller structure, such as K_f, K_r, l_f, l_r and I_{zz}, also correspond to a Mercedes S Class. Figure 32 shows the Nyquist and Bode plots of the corresponding $\tilde{\gamma}(s)$.
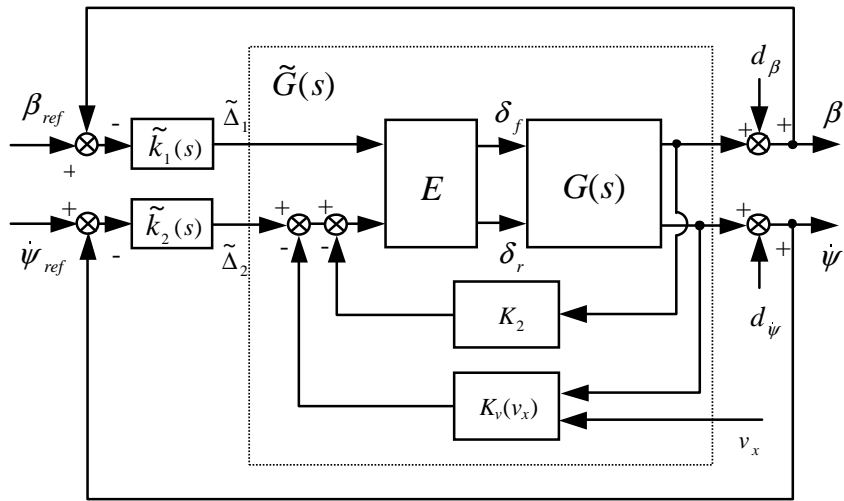
Figure 30: Multivariable control design problem in terms of $\tilde{G}(s)$
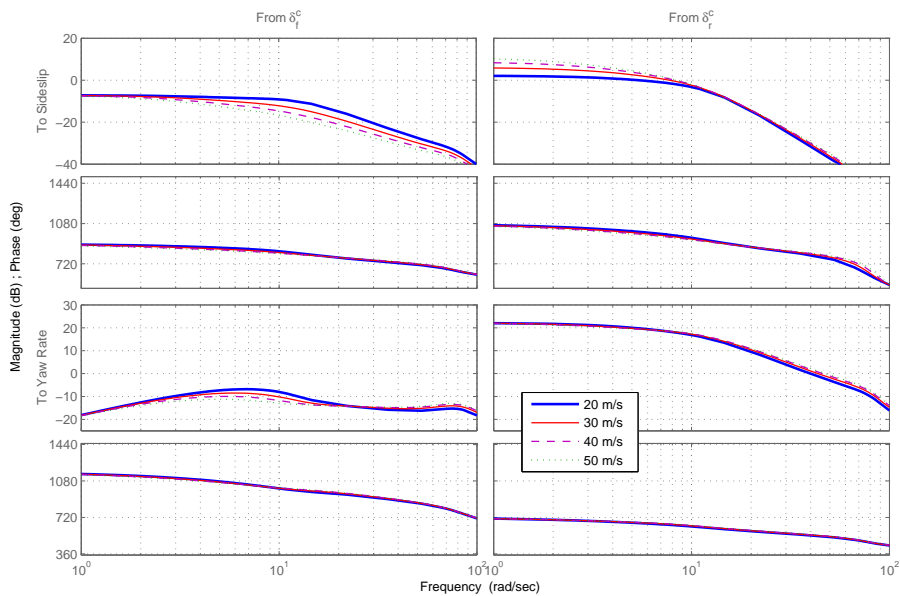

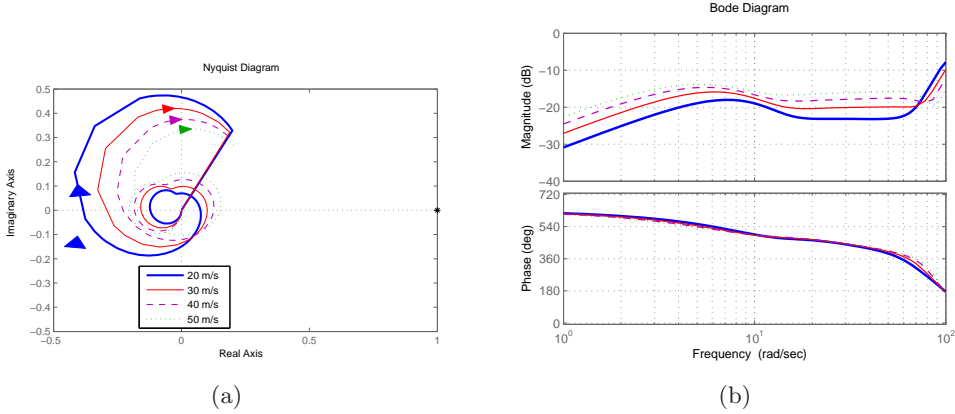Figure 31: Bode plot of $\tilde{G}(s)$ for different vehicle speeds

Figure 32: Nyquist plot and Bode diagram of $\tilde{\gamma}(s)$ for different vehicle speeds

To generate the plots in Figures 31, and 32 the values of the parameters in the controller structure has been set to those obtained from the design process outlined below. As it can be seen in the figures, $\tilde{G}(s)$ is not exactly upper-triangular. This is due to the additional dynamics in $G(s)$—time delay, actuators, tyre force and caster dynamics—that are not present in the ideal model $G^i(s)$. However, it can be assumed that $\tilde{\gamma}(s)$ and $\tilde{g}_{21}(s)$ are small enough to be negligible up to a certain frequency. In Figure 31 it can be seen that the yaw rate dynamics are not strictly speed-invariant but they can be considered so up to a certain frequency. Similarly, the sideslip dynamics are not speed-invariant but they can be considered so up to a certain frequency, which is lower than for the yaw rate. Thus, providing that the open-loop bandwidth of channel 2 (yaw rate) is approximately 10 rad/s and that the one of channel 1 (sideslip) is kept below 2 rad/s it would be possible to design two linear controllers $\tilde{k}_1(s)$ and $\tilde{k}_2(s)$ valid for virtually any vehicle speed. In addition, the bandwidth separation between the two channels would contribute to mitigate the unbalance in the plant and improve the cross-channel disturbance rejection of the system from sideslip to yaw rate.

The proposed controller structure resolves the problem posed by the RHPZ in $g_{11}(s)$. Neither of the two diagonal elements $\tilde{g}_{11}(s)$ and $\tilde{g}_{22}(s)$ have RHPZs and, consequently, the integrity of the control system in Figure 30 with respect to loop failure is not compromised. Both off-diagonal elements now have a RHPZ, but, in principle, these zeros do not pose any limitations to the system performance, robustness or integrity.

Outline of the design process Details on the design of the controllers $\tilde{k}_1(s)$ and $\tilde{k}_2(s)$ can be found in [36]. Here it is provided a summary of the design process. Before actually designing $\tilde{k}_1$ and $\tilde{k}_2$, two tasks have to be carried out:

1. In order to improve the cross-channel disturbance rejection in the sideslip channel (disturbances from the reference yaw rate to the sideslip response) and the overall robustness of the control system, a low-pass filter is added to

the cross-feedback term. This results in K_2 in Figure 30 taking the form:

$$K_2(s) = \left(1 - \frac{K_r l_r}{K_f l_f}\right) \frac{1}{\frac{s}{s_0} + 1} \tag{149}$$

where the value of the pole frequency, s_0, is to be selected.

2. The value of v_{x0} in $K_v(v_x)$ has to be chosen. The choice of v_{x0} is related to the robustness of the system.

Once s_0 and v_{x0} have been selected, we can write the transfer function matrix $\tilde{G}(s)$ for any given vehicle speed. As mentioned above, by imposing a bandwidth separation between the two channels, the controllers $\tilde{k}_1(s)$ and $\tilde{k}_2(s)$ can be designed based on $\tilde{g}_{11}(s)$ and $\tilde{g}_{22}(s)$, respectively, using classical Bode plot-based SISO techniques. Simple controllers of the form

$$\tilde{k}_1(s) = -\frac{K_{1I}}{s}, \quad \text{Integrator} \tag{150}$$

$$\tilde{k}_2(s) = K_{2p} + \frac{K_{2I}}{s}, \quad \text{PI controller} \tag{151}$$

$$\tag{152}$$

achieve satisfactory performance regarding the rejection of cross-channel and external disturbances. These controllers result in a low bandwidth sideslip channel (approx 1 rad/s) and a high bandwidth yaw rate channel (approx 10 rad/s). The speed-dependent feedback term $K_v(v_x)$ acts as an implicit gain scheduling scheme that combines linear controllers parameterised by the vehicle speed into a non-linear controller valid for varying speed.

Figure 33 shows the Bode plots of the resulting channel transmittances —which are approximated by $\tilde{k}_1(s)\tilde{g}_{11}(s)$ and $\tilde{k}_2(s)\tilde{g}_{22}(s)$, respectively, since $\gamma(s)$ is small— for different vehicle speeds. It can be observed that both transmittances show almost no variation with speed for frequencies below the gain crossover.
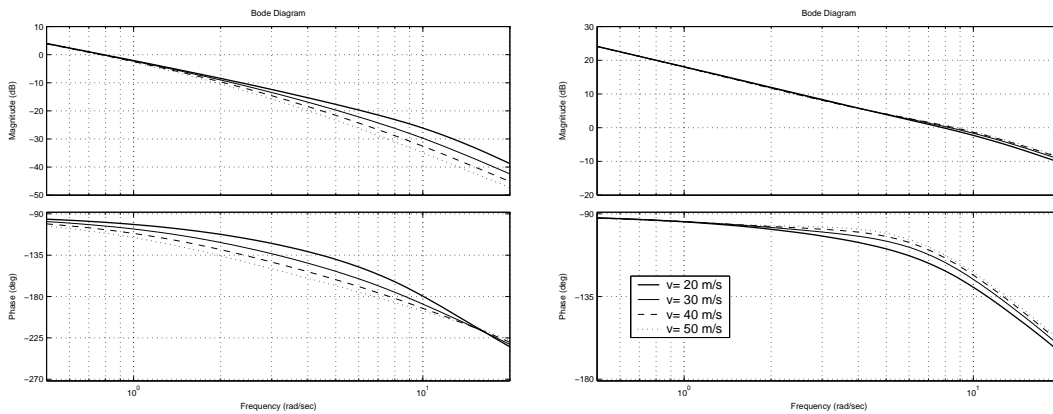

Figure 33: Bode plots of $\tilde{k}_1(s)\tilde{g}_{11}(s)$ and $\tilde{k}_2(s)\tilde{g}_{22}(s)$ for different vehicle speeds.

Having designed $\tilde{k}_1(s)$ and $\tilde{k}_2(s)$ to achieve robustness and disturbance rejection performance, we then add a linear feedforward element to the steering controller

Figure 34: Control system with the feedforward element

to improve its tracking performance. The feedforward, which is depicted in Figure 34, is made up of three elements: $F_\beta(s)$ and $F_{\dot\psi}(s)$, which speed up and shape the responses to reference signals,and $F_{\dot\psi\beta}(s)$, which improves the cross-channel disturbance rejection from yaw rate to sideslip.

6 Conclusions

In this report, the the theory and methods of controller design as they relate to the application work packages 1 and 2 of the CEMACSproject have been presented. The design framework has been developed, implemented and tested. The methodologies employed was ultimately driven by the need to meet the requirements of the application work packages as they evolved throughout the project.

References

[1] B. C. Chen and H. Peng, "A real-time rollover threat index for sports utility vehicles," in *Proceedings of the American Control Conference*, 1999.

[2] B. C. Chen and H. Peng, "Rollover prevention for sports utility vehicles with human-in-the-loop evaluations," in *5th Int'l Symposium on Advanced Vehicle Control*, 2000.

[3] C. R. Carlson and J. C. Gerdes, "Optimal rollover prevention with steer by wire and differential braking," in *Proceedings of the ASME International Mechanical Engineering Congress and Exposition*, (Washington, D.C. USA), 2003.

[4] D. Odenthal, T. Bunte, and J. Ackermann, "Nonlinear steering and braking control for vehicle rollover avoidance," 1999.

[5] H. B. Pacejka, *Tyre and Vehice Dynamics*. Butterworth Heinemann, 2002.

[6] J. Y. Wong, *Theory of Ground Vehicles*. John Wiley and Sons, second ed., 1993.

[7] J. Svendenius, "Tire models for use in braking applications," Licentiate Thesis ISRN LUTFD2/TFRT--3232--SE, Department of Automatic Control, Lund University, Sweden, Nov. 2003.

[8] P. Tøndel and T. A. Johansen, "Control allocation for yaw stabilization in automotive vehicles using multiparametric nonlinear programming," in *American Control Conference*, 2005.

[9] B. Johansson and M. Gäfvert, "Untripped suv rollover detection and prevention," in *43rd IEEE Conference on Decision and Control*, 2004.

[10] E. Dahlberg, *Commercial Vehicle Stability - Focusing on Rollover*. PhD thesis, Royal Institute of Technology, Stockholm, Sweden, 2001.

[11] O. Härkegård, *Backstepping and Control Allocation with Applications to Flight Control*. PhD thesis, Department of Electrical Engineering, Linköping University, SE–581 83 Linköping, Sweden, May 2003.

[12] G. Bevan, H. Gollee, and J. O'Reilly, "Automatic lateral emergency collision avoidance for a passenger car," *Int J Control*, 2006. submitted for publication.

[13] "ISO 3888 passenger cars - test track for a severe lane-change manoeuvre – part 1: Double lane-change," 1999.

[14] "ISO 3888 passenger cars - test track for a severe lane-change manoeuvre – part 2: Obstacle avoidance," 2002.

[15] J. Ackermann, J. Guldner, W. Sienel, R. Steinhauser, and V. Utkin, "Linear and nonlinear controller design for robust automatic steering," *IEEE Transactions of Control Systems Technology*, vol. 3, no. 1, pp. 132–143, 1995.

[16] J. Ackermann, D. Odenthal, and T. Bünte, "Adventages of active steering for vehicle," *in 32nd International Symposium on Automotice Technology and Automation*, pp. 263–270, 1999.

[17] J. Ackermann and T. Bünte, "Yaw disturbance attenuation by robust decoupling of car steering," *Control Eng. Practice*, vol. 5, no. 8, pp. 1131–1136, 1997.

[18] S. Mammer and D. Koenig, "Vehicle handeling improvement by actice steering," *Vehicle System Dynamics*, vol. 38, no. 3, pp. 211–242, 2002.

[19] .-., "Handeling improvement of robust car steering," *in International COnference on Adcances in Vehicle Control and Safety*, 1998.

[20] A. T. van Zanten, R. Erhart, and G. Pfaff, "The vehicle dynamics control system of BOSCH," *SAE 950759*, 1995.

[21] V. Alberti and E. Babbel, "Improved driving stability of active braking of the individual wheels," *In Proc. of the International Symposium on Advanced Vehicle Control*, pp. 717–732, 1996.

[22] T. Shim and D. Margolis, "Using μ feedforward for vehicle stability enhancement," *Vehicle System Dynamics*, vol. 35, no. 2, pp. 113–119, 2001.

[23] T. A. Johansen, "Optimizing nonlinear control allocation," *Proc. IEEE Conf. Decision and Control. Bahamas*, pp. 3435–3440, 2004.

[24] J. Tjønnås and T. A. Johansen, "Adaptive optimizing nonlinear control allocation," *In Proc. of the 16th IFAC World Congress, Prague, Czech Republic*, 2005.

[25] Y. Hattori, K. Koibuchi, and T. Yokoyama, "Force and moment control with nonlinear optimum distribution of vehicle dynamics," *in Proc. of the 6th International Symposium on Advanced Vehicle Control*, pp. 595–600, 2002.

[26] J. H. Plumlee, D. M. Bevly, and A. S. Hodel, "Control of a ground vehicle using quadratic programming based control allocation techniques," *in Proc. American Contr. Conf.*, pp. 4704–4709, 2004.

[27] P. Tøndel and T. A. Johansen, "Control allocation for yaw stabilization in automotive vehicles using multiparametric nonlinear programming," *American Control Conference*, 2005.

[28] U. Kiencke and L. Nielsen, *Automotive Control Systems*. Springer-Verlag, 2000.

[29] J. Ackermann, "Robust decoupling, ideal steering dynamics and yaw stabilization of 4ws cars," *Automatica*, vol. 30, pp. 1761–1768, 1994.

[30] G. Genta, *Motor Vehicle Dynamics, Modeling and Simulation*. World Scientific, 1997.

[31] T. D. Gillespie, *Fundamentals of vehicle dynamics*. Society of Automotive Engineers, 1992.

[32] W. Leithead and J. O'Reilly, "Multivariable control by individual channel design," *International Journal of Control*, vol. 54, no. 1, 1991.

[33] W. Leithead and J. O'Reilly, "'m-input m-output' feedback control by individual channel design - part 1: Structural issues.," *International Journal of Control*, vol. 56, 1992.

[34] W. Leithead and J. O'Reilly, "Performance issues in the individual channel design of 2-input 2-output systems - part 1: Structural issues.," *International Journal of Control*, vol. 54, 1991.

[35] W. Leithead and J. O'Reilly, "Performance issues in the individual channel design of 2-input 2-output systems - part 3: Non-diagonal control and related issues.," *International Journal of Control*, vol. 55, 1992.

[36] M. Vilaplana, D. Leith, W. Leithead, and J. Kalkkuhl, "Control of sideslip and yaw rate in cars equipped with 4-wheel steer-by-wire," in *Proceedings of the 2004 SAE Automotive Dynamics, Stability and Controls Conference*, pp. 143–153, 2004. SAE Paper No. 2004-01-2076.